

# Ages for Globular Clusters in the Outer Galactic Halo: The Second Parameter Clusters Palomar 3, Palomar 4 and Eridanus<sup>1</sup>

Peter B. Stetson

Dominion Astrophysical Observatory, Herzberg Institute of Astrophysics, National Research Council, 5071 West Saanich Road, Victoria, British Columbia V8X 4M6, Canada

Electronic mail: peter.stetson@hia.nrc.ca

Michael Bolte

UCO/Lick Observatory and the Department of Astronomy and Astrophysics, University of California, Santa Cruz, California 95064

Electronic mail: bolte@lick.ucolick.org

William E. Harris

Department of Physics, McMaster University, Hamilton, Ontario L8S 4M1, Canada

Electronic mail: harris@physics.mcmaster.ca

James E. Hesser and Sidney van den Bergh

Dominion Astrophysical Observatory, Herzberg Institute of Astrophysics, National Research Council, 5071 West Saanich Road, Victoria, British Columbia V8X 4M6, Canada

Electronic mail: james.hesser@hia.nrc.ca, sidney.vandenbergh@hia.nrc.ca

Don A. Vandenberg

University of Victoria, Department of Physics & Astronomy, PO Box 3055, Victoria, British Columbia V8W 3P7

Electronic mail: davb@uvvm.uvic.ca

---

<sup>1</sup> Based on observations made with the NASA/ESA *Hubble Space Telescope*, obtained at the Space Telescope Science Institute, which is operated by the Association of Universities for Research in Astronomy, Inc., under NASA contract NAS5-26555.

Roger A. Bell

University of Maryland, Department of Astronomy, College Park MD 20742-2421

Electronic mail: rabell@astro.umd.edu

Jennifer A. Johnson

UCO/Lick Observatory and the Department of Astronomy and Astrophysics, University of

California, Santa Cruz, California 95064

Electronic mail: jennifer@lick.ucolick.org

Howard E. Bond and Laura K. Fullton

Space Telescope Science Institute, 3700 San Martin Drive, Baltimore MD 21218

Electronic mail: bond@stsci.edu, fullton@stsci.edu

Gregory G. Fahlman and Harvey B. Richer

Department of Physics & Astronomy, University of British Columbia, Vancouver, British

Columbia V6T 1Z4

Electronic mail: richer@astro.ubc.ca, fahlman@astro.ubc.ca

Received \_\_\_\_\_; accepted \_\_\_\_\_

## ABSTRACT

We have used the WFPC2 camera on the *Hubble Space Telescope* to obtain photometry of the outer-halo globular clusters Palomar 3, Palomar 4, and Eridanus. These three are classic examples of the “second parameter” anomaly because of their red horizontal-branch morphologies in combination with their low-to-intermediate metallicities. Our color-magnitude diagrams in  $(V, V-I)$  reach  $V_{lim} \simeq 27.0$ , clearly delineating the subgiant and turnoff regions and about three magnitudes of the unevolved main sequences. The slopes and dereddened colors of the giant branches are consistent with published  $[\text{Fe}/\text{H}]$  estimates that rank the clusters (Pal 3, Eridanus, Pal 4) in order of increasing metallicity, with all three falling near or between the abundance values of the classic nearby halo clusters M3 and M5. Differential fits of their color-magnitude diagrams are made to each other and to M3 and M5 for relative age determinations. We find that the three outer-halo cluster CMDs differ from the nearby clusters in a way that is consistent with their being younger by  $\sim 1.5 - 2$  Gyr, if we have correctly estimated the clusters’ chemical-abundance ratios. Conversely, the inferred age difference could be smaller ( $\lesssim 1$  Gyr) if either  $[\text{Fe}/\text{H}]$  or  $[\alpha/\text{Fe}]$  for the outer-halo clusters is significantly lower than we have assumed. Possible age spreads of order 1 Gyr among both the nearby and outer-halo clusters may also be present.

*Subject headings:* Globular clusters: individual (Palomar 3, Palomar 4, Eridanus); Galaxy: formation

## 1. Introduction

This is the second paper in which we report results of age measurements for the globular clusters at the outermost reaches of the Milky Way halo. In the first paper of this series (Harris *et al.* 1997 [Paper I]), we showed that the massive globular cluster NGC 2419, at a Galactocentric distance of  $\sim 90$  kpc, has a color-magnitude diagram (“CMD”) that is indistinguishable from that of M 92 and other nearby halo clusters with the lowest known metallicities,  $[\text{Fe}/\text{H}] \simeq -2.2$ . These clusters have the same age to within the measurement precision of  $\simeq 1$  Gyr, suggesting that globular cluster formation may have *started* at virtually the same time everywhere across the entire expanse of the protoGalaxy.

However, NGC 2419 represents only the upper envelope of the chronology of the outermost-halo clusters. The other remote clusters (Palomar 3, 4, 14, Eridanus, and AM-1) are intriguing in quite a different way as strong cases of the classical “second parameter” problem: their horizontal-branch (“HB”) morphology is redder than the mean for nearby halo clusters of similar (low to intermediate)  $[\text{Fe}/\text{H}]$ . The tendency for the second-parameter effect to become increasingly evident in the outer halo is one of the key motivations behind the Searle & Zinn (1978 [SZ]) scenario in which the Galaxy’s spherical halo is envisaged as having accumulated over time in a series of mergers of sub-galactic fragments. Making the plausible assumption that age is the most important second parameter responsible for intrinsic scatter in the relation between  $[\text{Fe}/\text{H}]$  and HB morphology, SZ concluded that the mean age of the clusters decreases, and the age spread increases with increasing Galactocentric distance,  $R_{\text{GC}}$ . By contrast, if all parts of the spherical halo formed into stars during a rapid free-fall collapse as was argued by Eggen, Lynden-Bell & Sandage (1962 [ELS]), it would be much more likely that the halo clusters would have rather similar ages and would (for example) follow a simple relation between CMD morphology and metallicity.

Arguing from a comparison of quantitative simulations of HB morphology as a function

of metal abundance and age to CMDs of real clusters Lee, Demarque & Zinn (1994, hereinafter LDZ; see especially their Fig. 7) concluded that the globular clusters within  $\sim 8$  kpc of the Galactic center — spanning the full metal-abundance range from less than one one-hundredth solar to nearly the solar value — are essentially coeval. Those at Galactocentric distances between 8 and 40 kpc formed an average of some 2 Gyr later, but with a perceptible dispersion in their formation epochs. Finally, the five Galactic globulars with red horizontal branches that lie outside 40 kpc formed more than 4 Gyr later than their counterparts in the Galactic center (these statements are based upon our interpretation of LDZ’s Fig. 7).

Lee (1992) has added another wrinkle to the earliest formation history of the Galaxy, using another argument based on HB morphology. He notes that the RR Lyrae variables in Baade’s window — a region where we are allowed a more or less clear glimpse into the Galactic bulge — possess metal abundances closely bunched about a value of  $[\text{Fe}/\text{H}] = -1.0$ . He then argued that for stars of such high metal abundance to populate the HB instability strip, they must be  $\sim 1$  Gyr older than even the mean age of the globular clusters with  $R_{\text{GC}} < 8$  kpc.

However, the foregoing arguments rely on the assumptions that age is the *dominant* second parameter after metal abundance, and that HB morphology can be used in a simple and direct way as a measure of cluster age. These assumptions are straightforward and widely accepted, but they are perhaps not yet ironclad, and the debate continues (*e.g.*, Stetson, Vandenberg & Bolte 1996; Sarajedini, Chaboyer & Demarque 1997). There are two additional steps required to test and calibrate this chronology directly: first, we must measure in considerable detail the chemical compositions of stars in these clusters (since composition differences can mimic age differences in a variety of ways); and second, we must make much more direct estimates of age based on photometry of the main sequence

and subgiant branch in clusters spanning the range of Galactic environments. Stars in these stages of evolution are driven by somewhat simpler internal physics, and suffer from fewer potential complications due to uncertain mid-life processes such as mixing and mass-loss, than the HB stars (see, *e.g.*, Sweigart 1997).

Among the six Galactic globular clusters at Galactocentric distances greater than (to choose an arbitrary boundary) that of the Large Magellanic Cloud, only one — Pal 14 — has had its main-sequence turnoff detected from the ground (Sarajedini 1997), although even in this best case the data penetrate less than a magnitude past the turnoff. Sarajedini argues that Pal 14, with  $[\text{Fe}/\text{H}] \approx -1.6$ , is 2 Gyr younger than the nearby globular M 5 and 4 Gyr younger than NGC 6752. Additional caveats on these results are that M 5 may have a significantly higher  $[\text{Fe}/\text{H}]$  than Pal 14, and NGC 6752 has an extremely blue HB morphology that makes it very difficult to register it and Pal 14 to a common distance modulus.

It is possible that the outermost-halo objects may actually bear little direct relevance to the formation history of the main part of the Galaxy. Many or all of the red-HB clusters in particular (Pal 3, 4, 14, Eridanus, AM-1) may belong to a stream of remote satellites (the Fornax-Leo-Sculptor stream; see Majewski 1994) in an orbital plane with an extremely large semimajor axis,  $R \sim 150$  kpc or more. No matter whether the Galaxy itself formed in a monolithic *or* a hierarchical fashion, it is possible that this handful of objects was born well apart from the original protoGalaxy, and are now left orbiting a large stellar system of which they were never really an integral part. If this is true, these clusters may merely be a red herring in the search for clues to the formation of the Milky Way. But at least these same clusters should still provide us with a test of the proposed correlation between HB morphology and age, which is currently regarded as the essence of the second-parameter problem. In this paper, we use data from the *Hubble Space Telescope* to address the

questions of *whether*, and *to what extent*, the intermediate-metallicity clusters of the outer halo and the nearby halo really do have different ages. (Following LDZ, we separate the “inner” halo from the “intermediate” halo at a Galactocentric distance of about  $R_{\odot}$ , and the “intermediate” from the “outer” halo at about 50 kpc. In this paper, we use the word “nearby” in its common English sense, to describe those clusters that are close to the Sun and, hence, usually quite well studied. It encompasses some of the outermost members of the inner halo as well as the closer members of the intermediate halo; “nearby clusters” without the additional modifier “halo” can also include a few of the nearer disk and/or bulge clusters.)

## 2. Observations and Data Reduction

The clusters we report on here are Palomar 3, Palomar 4,<sup>2</sup> and Eridanus. These are three of the six known globulars beyond a Galactocentric distance  $R_{GC} \sim 50$  kpc, and (typically for such objects) have low luminosities, diffuse structures, and low to intermediate [Fe/H] values. Pal 3 and Pal 4 were imaged with the WFPC2 camera during *HST* Cycle 4, with Pal 4 being visited twice. Eridanus was observed during Cycle 5. As was the case for NGC 2419, the first visit to Pal 4 resulted in eight long exposures in F555W (each of 1400 s duration) and F814W (of 1300 s), after which the spacecraft was shifted by 20'' toward the center of the cluster, and six short exposures were taken in each filter (60 s in F555W and 30 s in F814W). For the second visit to Pal 4 and the visit to Pal 3, a different scheme was employed. For these observations we specified that the cluster be

---

<sup>2</sup>Results from preliminary analyses of the present data for Pal 3 and Pal 4 were included in the study by Richer *et al.* (1996). The current analysis supersedes the results cited in that paper.

centered on the PC1 chip and requested cycles of exposures, each cycle consisting of an (approximately) 1800 s, a 60 s, and a 30 s exposure; we obtained eight such cycles per filter for each cluster. Because Eridanus is closer than the other two clusters, for this system we obtained seven exposures of 1100 or 1200 s duration in each of F555W and F814W, plus  $3 \times 180$  s in F555W and  $3 \times 230$  s in F814W. Extensive additional details about these observations may be obtained by electronic query to either the Space Telescope Science Institute in Baltimore (<http://archive.stsci.edu/HDA/>), or the Canadian Astronomy Data Centre (<http://cadwww.hia.nrc.ca/hst/science.html>; specify GO programs 5481, 5672, and 6106: J. E. Hesser, PI), or by contacting the first author of this paper.

The process of data reduction was the same as that for NGC 2419 in Paper I, and will be described more completely in Stetson (1998, in preparation). The suite of codes collectively referred to as the third-generation DAOPHOT (including ALLFRAME; see Stetson 1994) was employed to obtain instrumental magnitudes and colors for all measurable stars in the WFPC2 fields and to merge these onto a common photometric system. Raw observed instrumental magnitudes were corrected for charge loss due to charge-transfer inefficiency by an amount equal to  $-0.04$  mag per 800 pixels times the  $y$ -coordinate of the star on the chip (Holtzman *et al.* 1995; Whitmore & Heyer 1997). Color terms for the transformation from the instrumental (F555W, F814W) magnitude system to the standard Johnson  $V$ , Kron-Cousins  $I$  systems were taken directly from Holtzman *et al.* (their Table 7). The zero-point calibration relies ultimately on ground-based images of some of these same fields obtained by us. We found that the zero points inferred for our *short* exposures agree with those from Holtzman *et al.* to within  $\pm 0.02$  mag in both  $V$  and  $I$ . However, the zero points appropriate to our long exposures appear to differ from those of Holtzman *et al.* by some 0.05 mag in each filter, in the sense that the effective quantum efficiency of the CCDs in WFPC2 appears to be higher in long exposures than in short ones. We believe that this behavior is consistent with the notion that crystal-lattice imperfections in the CCDs act



as charge traps. In long exposures, where the diffuse sky foreground is appreciable, these traps consume electrons and lower the overall diffuse flux in the image without affecting stellar profiles or brightnesses. However, in short exposures the diffuse sky is not sufficient to fill all the traps, and electrons are consumed from the charge packets representing stellar images either during the exposure itself or during readout of the chip. This effect appears to operate *in addition* to the charge-transfer inefficiency ramp of  $-0.04$  mag per 800 pixels mentioned above. Fortunately, for the differential comparisons to be performed below accurate knowledge of the zero points is not essential: incorrect values will slightly falsify the distances and/or reddening values inferred for our clusters, but the relative age indicators will be unaffected. We hope to be able to improve the fundamental accuracy of our zero points once the charge-transfer inefficiency of the WFPC2 CCDs becomes better characterized. For our present purposes, separate photometric zero-points for the long and short exposure times have been determined by direct comparison to our ground-based observations of Pal 4 and NGC 2419.

Later, we will compare the results for these three clusters to our ground-based photometry for the nearby halo clusters M 3 and M 5. Data for M 3 were obtained during seven observing runs on four different telescopes between 1983 and 1994 (although the *I*-band data came from only two of those runs), while M 5 was observed during twelve runs on six different telescopes during the same time span (again the *I*-band data were from two of those runs). These data include the observing run analysed by Johnson & Bolte (1998), but the images have been independently reanalysed and recalibrated for the present study. All the data from the various runs were homogenized to a common photometric system — that of Landolt (1992) — as originally outlined some years ago by Stetson (1990, 1993). The present ground-based photometric system is anchored to a total of some 44 observing runs in *V* and 17 runs in *I*.

### 3. The Color-Magnitude Diagrams

Figs. 1–3

Figures 1 through 3 show the CMDs we have derived from the *HST* imagery for the remote clusters, Pal 3, Pal 4, and Eridanus. For each object, the data from the four WFPC2 chips have been combined. The narrowness of the red giant branches (“RGBs”) in all three CMDs is consistent with our expectation that the four WFPC2 CCDs and the long and short exposures have all been normalized to the same photometric system to within  $\sim \pm 0.01$  mag. We note that all three of the outer-halo clusters contain significant numbers of blue straggler stars (about a dozen such objects appear in each of Figs. 1–3).

Figs. 4 & 5

Figures 4 and 5 illustrate the ground-based color-magnitude diagrams for M 3 and M 5 that we will later compare to those of the outer-halo clusters. The present data for these clusters give results that are very similar to those of Johnson & Bolte (1998), with about twice the sample size.

Palomar 3 is the only outer-halo cluster in our study which appears to contain RR Lyrae variables. Three were found by Gratton & Ortolani (1984), who also identified one candidate Population II Cepheid; a fifth variable candidate, which had previously been noted by Burbidge & Sandage (1958), was considered to be non-variable by Gratton and Ortolani. One of Gratton & Ortolani’s RR Lyrae stars, their number 34, lies outside our field coverage, as does the candidate Cepheid (their number 102). We have recovered the other two candidate RR Lyraes from Gratton and Ortolani; their number 155 = our number 1-233, and their number 283 = our number 2-614. In addition, in contrast to the conclusion of Gratton and Ortolani, we find that the Burbidge-Sandage candidate = Gratton-Ortolani number 188 = our number 2-198, is indeed a real variable. Finally, we identify four

Fig. 6

additional RR Lyrae candidates not previously noted. In Figure 6 we present light-curve fragments from our data for these seven stars. Within the limitations of the available data, all seven of the variables appear to have the asymmetric sawtooth lightcurve characteristic

Table 1 of RR<sub>ab</sub>-type variables. Table 1 represents notional period estimates for the stars from these data (for our present crude purposes, we neglect the slight difference in phase between extrema as observed in the two photometric bandpasses). We think it most likely that for five of the seven candidate variables, three full cycles occurred between the two dates of observation, while for the other two, candidates 1-299 and 2-614, barely more than two cycles elapsed between the end of the first observing sequence and the start of the second. These assumptions yield virtually identical periods of 0.6 d for all seven of the RR Lyrae candidates. The possibility of four cycles having occurred for any of the variables, implying a period of order 0.44 d, can be ruled out by the absence of significant lightcurve overlap on either occasion, since on each date we obtained continuous data strings more than 0.48 d in length. Conversely, the possibility that some of the variable candidates underwent only two full cycles or less during the course of observations would imply periods of order 0.9 d, which are extremely rare among classical RR Lyraes. The mean magnitude and color of all seven candidates is indicated in Fig. 1 as  $\langle V \rangle = 20.49 \pm 0.027$ ,  $\langle V-I \rangle = 0.66 \pm 0.061$ . Among the non-variable stars in our Pal 3 sample, we count six in the neighborhood of the red horizontal branch, implying a horizontal-branch morphology index for this cluster of  $(B - R)/(B + V + R) = -6/13 = -0.5 \pm 0.2$ .

We have determined fiducial points for the principal CMD sequences in two ways. First, we simply calculated robust mean magnitudes and colors (after three iterations of sigma-clipping) in bin steps of  $\Delta V \simeq 0.2$  mag for the three outer-halo clusters, and in steps of 0.1 mag for M3 and M5. These mean points are shown as squares in Figures 7 through 11 and are listed in Table 2: columns 1 and 2 give the mean  $(V, V - I)$  values for the stars found in each bin, while the last three columns give the number of stars per bin retained in each of the three iterations. Notice that the bin steps are not strictly uniform in  $\Delta V$ , particularly along the upper giant branch, where the bin intervals and sizes are determined more strongly by the (patchy) distribution of RGB stars.

Second, we took D. A. Vandenberg’s latest set of theoretical isochrones and, regarding them as a set of numerical drafting splines likely to resemble an actual cluster locus more closely than, say, a low-order polynomial, fitted them directly to the original data. These isochrones are essentially the ones described in Paper I except that they now incorporate the latest neutrino cooling rates (Itoh *et al.* 1996), which result in a small increase in the derived core mass at the giant-branch tip ( $0.002\text{--}0.004 M_{\odot}$ ) and an increase of  $\sim 0.025$  mag in the corresponding HB luminosity. These changes are irrelevant for our immediate purposes. Some complications, such as the uncertain effects of convection and mixing on the derived radii for evolved stars, reddening, and the practical difficulty of accurately characterizing the relationship between colors on the Johnson/Kron-Cousins standard system and those obtained with a particular filter/detector combination, continue to constitute problems for the reliable *absolute* interpretation of CMDs (*e.g.*, Vandenberg 1998, in preparation). The magnitude and color zero-points of the isochrones employed here are based on the use of theoretical zero-age HB models as absolute luminosity fiducial points, but it turns out that our models are numerically consistent with a compromise between cluster distance estimates from the latest Hipparcos parallaxes for subdwarfs on the one hand (*e.g.*, Pont *et al.* 1998), and for RR Lyraes on the other (Fernley *et al.* 1998). Clearly, absolute cluster ages will be quite a strong function of one’s assumptions concerning the distance scale (see, *e.g.*, Chaboyer *et al.* 1998 and Gratton *et al.* 1997; also, Hendry 1997), but unless we are very unlucky age *differences* from direct cluster-to-cluster comparisons will be minimally affected.

We used theoretical isochrones for  $[\text{Fe}/\text{H}] = -1.14, -1.31, -1.41, -1.54,$  and  $-1.61$ ;  $[\alpha/\text{Fe}] = 0.0, +0.3,$  and  $+0.6$ ; and age = 8, 10, 12, 14, 16, and 18 Gyr. We numerically fitted *all* of these isochrones to the data for *each* of the clusters, allowing arbitrary vertical and horizontal shifts in each case. Isochrones were fitted to the actual cluster data (*i.e.*, *not* to the normal points), and the fits were carried out in the  $(I, V-I)$  plane, because in this

representation the subgiant branch is more strongly sloped than in the  $(V, V-I)$  diagram. Looked at in another way, if apparent magnitude is taken as the independent variable and color as the dependent one, then the long, flat subgiant branch characteristic of young ages becomes vertical in the function  $V-I = \text{Fn}(V)$ ; indeed, for very young ages the relationship can be multi-valued so the mapping between color and magnitude becomes equivocal. The relation  $V-I = \text{Fn}(I)$  is better behaved in this regard.

The fits were carried out using a robust maximum-likelihood scheme that considered the photometric uncertainty of each stellar measurement and reduced the relative weights of obvious outliers. This method (essentially the same as the one illustrated in Fig. 6 of Stetson 1987) is quite insensitive to the actual numbers and distribution of outliers, and is also robust against variations in the details of the weighting scheme. After all the isochrone fits had been done, the one isochrone which produced the highest maximum of this likelihood function was identified and adopted as representing the position and shape of the turnoff and subgiant region of the CMD. Note that in this procedure we imposed no *a priori* constraints on cluster distance, reddening, chemical abundance, or age within the parameter space spanned by these particular isochrones, nor do we intend to draw any immediate *a posteriori* conclusions concerning those parameters. At this point, all we want is to utilize the theoretical isochrones as a set of numerical curves describing the shape and position of the turnoff and subgiant branch in the CMD. That said, we note that the specific isochrones selected by the statistical procedure were, in fact, reasonable: the best matches were achieved with model metal abundances in the range  $-1.41 < [\text{Fe}/\text{H}] < -1.61$  and model ages  $\sim 14\text{--}16$  Gyr. We stress again that no great weight is to be placed on these numerical quantities, apart from a general sense of satisfaction that they are not unreasonable.

Having determined which isochrone best matches the appearance of the cluster

sequence within two magnitudes of the turnoff,  $I_{TO} - 2 < I < I_{TO} + 2$  mag (solid curves in Figs. 7–11), we then read out from the isochrones the magnitudes and colors corresponding to five points: (1) the turnoff, (2) the point on the subgiant branch that is precisely 0.10 mag redder than the turnoff, (3) the point on the subgiant branch that is 0.05 mag redder than the turnoff, and (4) and (5) the points on the upper main sequence that are precisely 0.05 and 0.10 mag redder than the turnoff. After the  $(I, V-I)$  locations of these fiducial points had been determined, the magnitudes were converted to their  $V$ -band equivalents. We present the apparent visual magnitudes of isochrone points (2) through (5), denoted by  $V_{+0.10}^-$ ,  $V_{+0.05}^-$ ,  $V_{+0.05}^+$ , and  $V_{+0.10}^+$ , respectively, in Table 3. For purposes of the present discussion, we took the turnoff of an isochrone to be given by the magnitude  $M_{I,TO}$  such that the  $(V-I)_o$  color of the isochrone at a point 0.2 mag more luminous than  $M_{I,TO}$  is exactly equal to the color at a point 0.2 mag less luminous than  $M_{I,TO}$ . The tabulated color on the fitted isochrone at  $M_{I,TO}$  was then taken as the turnoff color of the cluster. This definition was adopted to avoid uncertainty due to minor numerical glitches either in the theoretical evolution calculations or in the interpolation from evolutionary tracks to isochrones. However, we subsequently found that the turnoff color defined in this way agreed to within  $10^{-4}$  mag of the bluest color actually achieved on the isochrone, so it seems our concerns were exaggerated.

Table 3

VandenBerg, Bolte & Stetson (1990, “VBS”) suggested using the main-sequence point  $V_{+0.05}^+$  to effect the vertical registration of cluster sequences for estimating relative ages, while Chaboyer *et al.* (1996a) advocated the use of the subgiant-branch point  $V_{+0.05}^-$ . The advantages of estimating a fiducial point on the subgiant branch are, first, that the sequence is more nearly horizontal than the main sequence, and second, that the photometry for individual stars is likely to be more precise. A fiducial point on the main sequence has the advantage that it can be estimated from a much larger number of stars. Furthermore, the shape of the upper main sequence is “simpler,” both in the sense that

the high-order derivatives are smaller and in the sense that the overall shape of the upper main sequence is less sensitive to age, abundance, and uncertain details of stellar interiors than the morphology of the subgiant branch (*e.g.*, VBS Figs. 2 and 3). However valid these distinctions may be in general, with the present data sets both the subgiant-branch and main-sequence fiducial points lead to much the same relative shifts, as Table 3 shows, and hence ultimately to the same astrophysical conclusions. In fact, since the whole shape of the turnoff region has been fitted as a fixed unit, when the various fiducial points have been determined in this way all are determined to essentially the same level of precision, and it makes little difference whether subsequent analysis depends upon the turnoff magnitude or upon either of the subiant-branch or main-sequence fiducial points.

We note that the isochrone fits imply turnoff colors approximately 0.007 mag bluer than the bluest normal points given in Table 2; possibly this is because the nose of the turnoff is more pointed in the models than in reality, but it is also possible that it is a consequence of a different level of effectiveness in rejecting binaries and uncertain data in the two schemes. In either case, since it appears to be a constant effect (at a level of  $\pm 0.003$  mag or so), it is unimportant for differential comparisons among clusters provided care is taken to base those comparisons on one type of analysis at a time. Apart from this minor difference, we see generally excellent agreement between the traditionally defined normal points and the somewhat more novel isochrone fits, indicating that the latter method does provide a robust, impersonal, and repeatable method for establishing the position and morphology of a cluster locus from unbinned data.

### 3.1. Intercomparison of the Outer Halo Clusters

The first-order variations of our present isochrones with changes of age, overall metal

Figs. 12–14 abundance, and  $\alpha$ -element enhancement are illustrated in Figures 12–14, where we have

normalized a selection of isochrones according to the precepts of VBS: the isochrones are translated horizontally to match their turnoff colors (vertical short-dashed line), and then they are shifted vertically to register the point on the upper main sequence that lies exactly 0.05 mag redder than the turnoff (cross). The variation of isochrone morphology with a change in one of the assumed input parameters is then most easily perceived as a change in the position of the giant branch. For subsequent comparison with our cluster data, we have parameterized these morphology variations by the color difference between the turnoff and the point on the giant branch (horizontal long-dashed line) that is precisely 3.0 mag brighter in  $V$  than the upper-main-sequence fiducial registration point (cross); this corresponds to a magnitude level 2.19 or 2.20 mag brighter than the turnoff, as we have defined it above. We will represent this color difference by  $(V-I)_{GB} - (V-I)_{TO}$ , or  $\Delta(V-I)$ . Clearly, when isochrones are compared to cluster data or cluster sequences are compared to one another after registration in this fashion, the differential interpretations that one may then make are independent of cluster distance and reddening and of zero-point errors in both the photometry and the theoretical isochrones. We find that the change in giant-branch color associated with a change in presumed age  $\tau$  from 8 to 16 Gyr is  $\delta[\Delta(V-I)] = -0.115$  mag, or  $\delta[\Delta(V-I)]/\delta \log \tau = -0.382$  mag/dex, which — in first-order expansion about an age of 12 Gyr — corresponds to about  $-0.014$  mag/Gyr. Similarly, to first order  $\Delta(V-I)$  decreases by about 0.04 mag for a 1 dex increase in either  $[\text{Fe}/\text{H}]$  or  $[\alpha/\text{Fe}]$ .

The true cluster abundances  $[\text{Fe}/\text{H}]$  and  $[\alpha/\text{Fe}]$  are therefore significant for interpreting these data, and we discuss current estimates in detail in the Appendix. The literature values are not definitive, but they suggest that the three clusters are quite similar in  $[\text{Fe}/\text{H}]$ , but with Pal 3 likely to be the most metal-poor, Pal 4 the most metal-rich, and Eridanus nearly as metal-rich as (and perhaps indistinguishable from) Pal 4. In Figure 15 we compare the normal points of the three clusters after dereddening and registration of their HB levels (details to be discussed below). The reddening values  $E(B-V)$  are

Fig. 15



taken from Harris (1996), “Catalogue of Milky Way Globular Cluster Parameters” (see <http://www.physics.mcmaster.ca/Globular.html>, revision of 1997 May 15), and in our present analysis we have taken  $E(V-I) = 1.3E(B-V)$ . (This value comes from interpolation within Table 3 of Cardelli, Clayton & Mathis 1989, taking  $V \sim 555$  nm and  $I \sim 814$  nm; recall that the reddening actually occurs in the instrumental magnitudes and not in the standard ones. The reddening values estimated for these five clusters are so small and so similar that our results are quite insensitive to the value assumed for this ratio.) For purposes of this illustration only, we have assumed that all three clusters have an HB luminosity  $M_V = +0.70$  at  $(V-I)_o = 0.60$  (a color close to that of the turnoffs). This photometric comparison supports the conclusion that the clusters are indeed similar in  $[\text{Fe}/\text{H}]$  and that the relative metallicity ranking from the literature is probably correct: Pal 3 has the steepest and bluest RGB, while Eridanus and Pal 4 have RGBs with slightly redder colors and flatter slopes that are virtually identical to one another. In addition, the HB of Pal 3 extends blueward into the RR Lyrae instability strip, whereas the HBs for both Eridanus and Pal 4 are simply red stubs with extremely small ranges in color, which — all other things being equal — also tends to corroborate the inferred metallicity ranking.

The near-coincidence of the main-sequence turnoff (“MSTO”) and subgiant regions among all three clusters immediately suggests that they have similar ages. Figure 16 shows the three cluster fiducials after registration via the VBS method. After such registration, any age differences should be manifest as offsets in the cluster RGBs (again, all other things — such as composition — being equal). None is obvious in this diagram. However, we can perform a more quantitative test: Figure 17 shows the color-magnitude diagrams of Pal 3, Pal 4, and Eridanus with the three clusters registered to match their apparent turnoff colors and  $V_{+0.05}^+$  fiducial magnitudes derived from the isochrone fits (use of the fitted turnoff magnitudes or the  $V_{+0.05}^-$  fiducial points in effecting the vertical registration would have made no material difference to the comparison). To eliminate some poorer measurements,

here we consider only those stars with photometric uncertainties  $\sigma(V-I) < 0.05$  mag, where the standard error assigned to a given star represents a compromise between that derived from the expected Poisson and readout noise and that indicated by the actual frame-to-frame repeatability for that particular star; 13% of the measured stars were rejected by this criterion. After registration of the data, we fit a simple parabola to the color of the giant-branch stars as a function of visual magnitude for the three clusters taken together, over the range  $-4.1 < V - V_{+0.05}^+ < -2.0$  mag,  $|\delta(V-I)| < 0.07$  mag, where  $\delta(V-I)$  is the horizontal distance of a given point from the best-fitting parabola. This region is denoted by the curve-sided box in Fig. 17. Then the net offset of the data for each individual cluster from the fitted parabola was determined, as listed in Table 4: the table gives (column 2) the mean differential offset for the giant branch of each cluster, (column 3) the median offset among the giants for each cluster, (column 4) the standard deviation about the mean horizontal offset for the each cluster, (column 5) the number of stars contained in the box, and (column 6) the median value of  $\sigma(V-I)$  among the stars in the box. We note that the perceived standard deviation is quite a bit larger than our estimates of the photometric errors for the individual stars. There can be several reasons for this: (a) we may have underestimated our photometric errors; (b) there could be actual scatter among the giants in each cluster; (c) the giant branch might not be a perfect parabola over this range of magnitude; and (d) the derived standard deviation could be dominated by the random errors of stars with individual  $\sigma(V-I)$  values larger than the median value.

Table 4

Using the isochrones described above, we found that at  $[\text{Fe}/\text{H}] \approx -1.41$  and age  $\approx 12$  Gyr, the relationship between RGB color offset and age is  $\delta[\Delta(V-I)]/\delta\tau = -0.014$  mag/Gyr. If we take the relative giant-branch offset of Pal 3 and Pal 4 to be of order  $0.000 \pm 0.003$  mag, then we would argue that these clusters are coeval to a level of about 0.2 Gyr *if the difference in their abundances can be neglected* (although we will argue below that the abundance differences should *not* be neglected). On the other hand, the Eridanus

giant branch appears to be offset from the giant branches of the two Palomar clusters by some  $0.01 \pm 0.004$  mag, which would suggest that Eridanus is younger than the other two clusters by some  $0.7 \pm 0.3$  Gyr under the same set of assumptions.

It is also quite apparent in Fig. 17 that by aligning the three cluster sequences at the main-sequence fiducial magnitude  $V_{+0.05}^+$ , we have also brought the three clusters' HBs into excellent coincidence. The small number of HB stars in each cluster perhaps makes it dangerous to try to be overly quantitative (note in particular that the two double circles on the HB bluer than  $(V-I) - (V-I)_{TO} = 0.12$  represent mean values for two of the Pal 3 RR Lyrae variables; the other five were excluded by the  $\sigma(V-I) < 0.05$  criterion), we feel that we may conservatively estimate that the  $\Delta V_{TO}^{HB}$  values for the three clusters do not differ by more than 0.05 mag or so (we present actual measured values in Table 6 below). As our isochrones suggest that at  $[\text{Fe}/\text{H}] \approx -1.41$  and age  $\approx 12$  Gyr the turnoff fades by some +0.085 mag/Gyr in  $V$ , this would suggest an upper limit of some 0.6 Gyr for the total age spread among these clusters if their abundances are similar. On the other hand, it is commonly believed that at a fixed age the  $V$ -band luminosity of the HB decreases by an amount of order 0.2 mag for every 1 dex increase in the overall heavy-element abundance (*e.g.*, Dorman 1993; Chaboyer, Demarque & Sarajedini 1996*b*; Gratton *et al.* 1997; our theoretical models are consistent with this: Vandenberg *et al.*, in preparation). If this is true, and if Pal 3 is of order 0.2 dex more metal poor than Pal 4 and Eridanus, then its HB should be of order 0.04 mag more luminous than in those other clusters. As we will discuss below, we believe that an offset of this order of magnitude is within the measuring error of the HB magnitude.

### 3.2. Comparison with the Near-Halo Clusters M 5 and M 3

With the CMD data for these three clusters we are in a position to begin answering a two-decades-old question: are the outer halo clusters with anomalously red HB morphologies truly younger than their counterparts in the nearby halo? Even with these data from *HST*, the answer to this question will depend on the estimates of the abundances of the outer halo clusters as well as for our representatives of the nearby halo, M 3 and M 5. (M 5 is currently inside the 8 kpc boundary that nominally separates the inner halo from the intermediate halo, but its large proper motion — Cudworth & Hanson 1993 — indicates that this situation is only temporary.) From the arguments presented in the Appendix, we believe that it is adequate at present to consider that Pal 4, Eridanus, and M 5 have essentially the same metallicity, while the metal abundances of Pal 3 and M 3 are similar to each other and perceptibly lower than those of the other three clusters.

While the principal sequences of the intermediate-halo clusters M 3 and M 5 can be compared to those of the outer-halo clusters by the same techniques as we have just applied to the comparison of the outer-halo clusters among themselves, it is best to remember that there are some underlying differences. The comparisons among the outer-halo clusters are direct: the observations were made with the same telescope (*HST*) and camera (WFPC2), and were subjected to an identical analysis and calibration procedure. M 3 and M 5, in contrast, were each observed with several different ground-based telescopes and on numerous occasions. Still, in many cases both clusters were observed on the same nights, and all observations have been referred to a common photometric system with the utmost rigor currently possible. However unlikely, there remains the possibility of some undetected difference between the *HST* and ground-based photometric systems that will render a comparison of the nearby halo clusters to the outer-halo ones less robust than comparisons that are strictly internal to either data set. Uncertainties in the *zero points* of the color

and magnitude scales are not of immediate concern; what might cause a significant problem would be uncorrected *color dependences* in the transformations from the instrumental to the standard magnitude systems, or a nonlinearity in the magnitude scale of either the space- or ground-based photometry. We stress that at present we have no evidence that such problems exist. Nevertheless, it would be wise to retain an extra quantum of skepticism in the backs of our minds as we interpret the comparison of the *HST* data to the ground-based observations.

We have repeated the determination of the relative giant-branch shifts for the five clusters just as in the previous section. This time we combined the rectified  $(V, V-I)$  data for all five clusters and refit the mean giant-branch parabola using the same constraints as before:  $-4.1 < V-V_{+0.05}^+ < -2.0$ ,  $|\delta(V-I)| < 0.07$ . We were a little more stringent in our selection of stars for M 3 and M 5, retaining only those stars with individual color errors  $\sigma(V-I) < 0.03$  mag. After the parabola had been fit, we determined the net offsets and scatter for each of the individual clusters relative to the mean giant branch of all of them as before; the results are listed in Table 5. The implications are that, if Pal 4, Eridanus, and M 5 all have the same composition — and we stress again that this means both  $[\text{Fe}/\text{H}]$  and  $[\alpha/\text{Fe}]$  — then Pal 4 and Eridanus are younger than M 5 by some 1.4 and 2.1 Gyr, respectively. The difference between Pal 3 and M 3 — again, assuming that these two clusters have the same chemical abundances — is similar: the net relative giant branch offset would imply that Pal 3 is younger than M 3 by some 1.7 Gyr.

Table 5

The alternative technique of determining the relative ages of clusters from the magnitude differences between their HBs and their main-sequence turnoffs requires a robust, consistent measurement of their HB magnitudes as well as of their turnoffs. The upper-main-sequence and subgiant-branch fiducial points given in Table 3 serve the latter purpose; now it remains to try to estimate the fiducial HB magnitudes with similar rigor.

We have computed zero-age horizontal branches (ZAHBs) consistent with the predictions of these main-sequence and giant-branch evolutionary tracks. We have employed them much as we used the isochrones in §3, simply as drafting splines of approximately the right shape to match the shape of an actual cluster HB. For comparison with Pal 3 and M 3, we have adopted theoretical ZAHB sequences with  $[\text{Fe}/\text{H}] = -1.54$ ,  $[\alpha/\text{Fe}] = +0.3$ , and  $Y = 0.2362$ ; Pal 4, Eridanus, and M 5 were compared to theoretical curves with  $[\text{Fe}/\text{H}] = -1.41$ ,  $[\alpha/\text{Fe}] = +0.3$ , and  $Y = 0.2366$ . Unlike the case with the turnoff isochrones, in this case we have allowed no freedom for horizontal translation of the theoretical curves, but have adopted their predicted colors and estimated reddening values verbatim, and have performed vertical shifts only in matching the theoretical ZAHBs to the lower envelope of the dereddened

Fig. 18 cluster data. Figure 18 shows these comparisons. The apparent visual magnitude of the fitted ZAHB was read out at an intrinsic color of  $(V-I)_o = 0.60$ , and the resulting  $V_{HB}$

Table 6 values are listed in Table 6. The external accuracy of these derived HB magnitudes is clearly dependent upon the requirement that the theoretical models *accurately* reproduce the luminosity variation of the HB with color, both at the red end (for the three outer-halo clusters), and at the blue end (for the two nearby clusters): if these curves are seriously wrong in detail, errors in the vertical placement of the ZAHB of several hundredths of a magnitude could easily result.

The precision of the HB magnitudes is also plainly jeopardized by the small number of HB stars in each cluster. For the three distant systems, there is little more that can be done; these diagrams contain most of the HB stars that Nature has provided. For M 5, at least, we have a convenient check. Sandquist *et al.* (1996) have published  $(V, I)$  photometry for a large sample of stars in this cluster. Johnson & Bolte (1998) find some modest errors in the zero points and possibly the scale of the Sandquist *et al.* magnitudes and, based on our own analysis, we agree. However, considering only those stars common to the Sandquist *et al.* sample and our current data set with  $14.5 < V < 16.5$  — 60

stars in all — we find net differences of  $\Delta V = +0.009 \pm 0.0029$  mag (standard error of the mean,  $\pm 0.022$  standard deviation of one difference) and  $\Delta I = -0.006 \pm 0.0026$  mag (s.e.m.,  $\pm 0.020$ , s.d.) in the sense (present – Sandquist *et al.*). The data of Sandquist *et al.* for stars with  $\sigma(V-I) < 0.03$  mag and lying more than  $96''$  from the center of M 5 are

Fig. 19 plotted, after correction for these offsets, in Figure 19 along with the same fitted ZAHB as before. [Note that here  $(m-M)_V$  does *not* necessarily mean  $-5 + 5 \log d(\text{pc}) + A_V$ ; rather it means  $m_V(\text{observed}) - M_V(\text{predicted})$ .] It seems that in this case, at least, our derived HB magnitude is consistent with the larger data set.

The last column of Table 6 lists the values of  $V_{TO} - V_{HB}$  that result from the difference between these HB magnitudes and the turnoff magnitudes derived from the isochrone fits. We see that for the three outer-halo clusters, the magnitude differences between the HB and the turnoff are nearly indistinguishable. Likewise, the difference between M 3 and M 5 is infinitesimal, but there is a difference of approximately 0.15 mag in the turnoff-to-HB magnitude difference (or the subgiant-branch-to-HB difference) between the nearby and remote clusters. In the approximation where all clusters have effectively the same chemical abundances, this would imply that the three outer-halo clusters are all roughly 1.5 – 2 Gyr younger than the two near-halo clusters.

To further quantify this conclusion, it is necessary to look more closely at the predictions of the current set of isochrones, in particular at the dependence of  $\Delta(V-I)$  and  $\Delta V$  on chemical abundance in comparison to their dependence on age. The solid curve in Figure 20 shows the predictions of Vandenberg’s isochrones for the evolution of the turnoff-to-giant-branch color difference (horizontal axis) and the turnoff-to-HB magnitude difference (vertical axis) as functions of age, from 8 to 18 Gyr, for abundances of  $[\text{Fe}/\text{H}] = -1.41$  and  $[\alpha/\text{Fe}] = +0.3$ . The horizontal tick marks intersect the curve at the model predictions for incremental age increases of 2 Gyr. The arrow illustrates the

Fig. 20

effect on the models produced by an assumed increase of +0.2 dex in either [Fe/H] or [O/Fe], according to this particular set of isochrones. There is considerable uncertainty in the horizontal placement of the solid curve in this diagram, as the predicted colors are dependent both upon uncertain details of convection theory and upon the assumed conversion from theoretical effective temperatures to observational colors. The slope of the curve could also be somewhat in error if the assumed dependence of convection or the temperature-to-color conversion on temperature itself is in error in a seriously non-linear fashion. Similarly, there could be some uncertainty in the absolute vertical positions of the tickmarks if the predicted HB luminosities are in error, or if the conversion of bolometric magnitudes to  $V$ -band magnitudes is incorrect for either the turnoff or HB stars. Therefore we particularly wish to de-emphasize any implication that we are measuring absolute ages for any of these clusters, at least until some of the remaining uncertainties in the model physics have been resolved. However, the size of the intervals between the vertical positions of the tick marks, representing increments of order 15–20% in age, should be relatively secure. The locations in this plane of the three outer-halo clusters are represented by open symbols, a triangle for Pal 3, a square for Pal 4, and a circle for Eridanus, while the two nearby clusters are indicated by filled symbols: a triangle for M 3 and a pentagon for M 5. Representative one-sigma error bars of  $\pm 0.005$  mag in  $\Delta(V-I)$  and  $\pm 0.05$  mag in  $\Delta V$  — due primarily to the uncertain placement of the HB lower envelope — are illustrated in the bottom right corner.

A consistent interpretation of the two age indicators can be made for the five clusters. *If we assume that the theoretical isochrones employed here correctly predict the dependence of  $\Delta V$  and  $\Delta(V-I)$  on age and chemical abundance*, then:

1. Those same models *slightly* (*i.e.*, by about 0.017 mag) overestimate the color difference between the giant branch and the turnoff, and the solid curve should be shifted as a



body to the left.

2. The data are consistent with an age difference of some 2 Gyr between M 3 and Pal 3 (Pal 3 younger) if their abundances are the same. Similarly, Pal 4 is of order 1.5 Gyr younger than M 5 if their abundances are identical.
3. The difference between the CMDs of Pal 4 and Eridanus could be due to
  - a. an age difference of somewhat less than 1 Gyr (Eridanus younger) if their abundances are the same; or
  - b. an abundance difference of some 0.2 dex with Eridanus being the more metal poor, in which case the age difference would be small.

The available spectroscopic data suggest that Eridanus *may* be some 0.14 dex more metal-poor than Pal 4, so the evidence for an age difference between the two is tenuous.

4. Even though the point for Pal 3 coincides with that for Pal 4 in this diagram, it is likely that Pal 3 is actually  $\sim 1$  Gyr older than Pal 4, because its point will have been displaced upward and to the right in this diagram as a result of its lower metal abundance.
5. Similarly, M 5 is almost certainly more metal-rich than M 3, so by the same argument as in point 4 above, M 5 must also be younger than M 3, probably by of order 1 Gyr or somewhat over.

#### 4. Discussion

The two relative age indicators,  $\Delta(V-I)$  and  $\Delta V$ , suggest a single self-consistent interpretation, namely that all three outer halo clusters are younger than their near-halo

counterparts by 1.5 to 2 Gyr, if we have correctly estimated the clusters’ chemical abundances. Sarajedini’s (1997) result for Pal 14 places this fourth outer-halo cluster in the same age ballpark (with, of course, the same caveats regarding uncertainties in the chemical abundance ratios and poorly understood processes in stellar interiors). Based on LDZ’s HB star models, if the red HB of Pal 3 is due to an age difference between this cluster and the average  $[\text{Fe}/\text{H}] \sim -1.5$  cluster in the near halo, Pal 3 is  $\sim 2$  Gyr younger than its near-halo counterparts. For Pal 4 and Eridanus, with HB types  $(B - R)/(B + V + R) = -1$ , Lee’s method can assign only a lower limit of  $\geq 2$  Gyr to the age difference, since the models for all ages younger than this imply wholly red HBs. These differential ages based on HB morphologies are in the same sense and of approximately the same size as those implied by our turnoff and subgiant comparisons.

Another angle from which to view this result is to ask, “What other parameters of the outer-halo clusters would have to be different if they are to have the *same* ages as the near-halo clusters?” We conclude that their age differences would be reduced to less than  $\sim 1$  Gyr (below which we would find it difficult to argue convincingly for genuine age differences) if we have overestimated the heavy-element abundances for the outer-halo objects — either  $[\text{Fe}/\text{H}]$  or  $[\alpha/\text{Fe}]$ , or a combination of the two — by 0.3 dex or more. We cannot rule out this possibility or, for that matter, less frequently discussed ones such as differences in helium abundance, mass loss rates on the giant branch, or stellar rotation. As we discuss in the Appendix, the  $[\text{Fe}/\text{H}]$  determinations for the outer-halo clusters are considerably weaker than those of the near-halo ones, and we have no quantitative information at all on their  $[\alpha/\text{Fe}]$  values. It is intriguing in this context that recent spectroscopic observations by Brown, Wallerstein & Zucker (1997) indicate that the young halo globular clusters Ruprecht 106 and Palomar 12 have relative oxygen and general  $\alpha$ -element abundances  $[\text{O}/\text{Fe}]$  and  $[\alpha/\text{Fe}] \sim 0.0$  to  $+0.1$ , in contrast to the value  $+0.3$  to  $+0.4$  observed in nearby, “normal” halo objects, although in the case of oxygen it is

unknown whether the abundance ratio in Rup 106 and Pal 12 is primordial or has been altered by mixing. If Pal 3, Pal 4, and Eridanus were to have primordial abundances  $[\alpha/\text{Fe}] \sim 0.0$ , then by basing our metallicity on measurements of Ca calibrated via nearby clusters with  $[\alpha/\text{Fe}] > 0$  we have assigned the wrong  $[\text{Fe}/\text{H}]$ . The sense of this error is such that it would reduce the inferred age difference between them and the near-halo clusters. We therefore believe it is of the utmost importance to obtain high-resolution spectroscopic data for the outer-halo clusters.

We have been scheduled observing time on *HST* to obtain color-magnitude diagrams for the last two remaining globular clusters beyond 50 kpc from the Galactic center, Palomar 14 and AM 1. At the same time, other research teams are using *HST* to pursue the study of the globular clusters near the Galactic center, and the dwarf galaxies that share the outer halo with the Palomar-like clusters, while still others are improving the available data for the near-halo objects. Thus, this is probably not the time to draw definitive conclusions regarding the early evolution of the Galactic spheroid. We can nevertheless draw some provisional conclusions that may be tested and rejected or refined by future work. As always, these conclusions are subject to the provisos that we have correctly estimated the chemical abundances of the objects under discussion and that no important physics has been omitted from the *differential* predictions of stellar evolution; simple errors in distance scale, convection theory, opacities, elementary particle physics, and anything else can be neglected provided they affect all globular clusters comparably, and provided we restrict ourselves to investigating the order and relative time intervals over which things happened, as opposed to the exact moment that any one event took place.

These results make a good case for age as a second parameter: the mean age of the outer-halo clusters with anomalously red HBs appears to be lower by  $\sim 1 - 2$  Gyr than that of the nearby, “normal” clusters. Although the original motivation for many programs

investigating ages for GGC has been to decide the mix of ELS and SZ that is required to match the cluster age distribution, it is clear that the GGC age distribution alone does not lead directly to a definitive formation scenario for the Galaxy. A range in GGC ages ( $>$  a few Gyr) is clearly inconsistent with the most naive version of a monolithic collapse model, but a general large-scale lumpy collapse accompanied or followed by various degrees of infall or accretion are allowed. Hierarchical formation models, like SZ, can more easily accommodate a range of ages than ELS, but they do not make *specific* predictions of the amount of time required to assemble the Galactic Halo and they do not predict an age distribution for GGC. Observationally, the Sagittarius dwarf spheroidal galaxy provides a striking example of a “late” accretion event that will add field stars and globular clusters to the Galaxy, yet not significantly alter the age dispersion of the GGC system. Still, it would be premature to conclude on the basis of the Sagittarius example that accretion was necessarily the sole, or even the dominant, mode of halo formation. Based on high-resolution simulations of the formation of galaxies after recombination (*e.g.*, Somerville & Primack 1998), there is a large overlap in the progenitor collapse times of objects that become galaxies of different masses. Objects that eventually become LMC-like galaxies can first start to form stars before, at the same time or after Milky Way-like objects. The age distribution is a crucial piece of the picture, but the final story will depend on other information such as detailed abundance patterns and kinematics for GGC halo populations (*e.g.*, Carney *et al.* 1997; Zinn 1993).

In contrast to theories that attempt to describe the hierarchical formation process of the Galaxy as a whole, the Harris & Pudritz (1994) formation model for the globular clusters themselves does make specific quantitative predictions for the amount of time required to assemble these systems within the outer Galactic halo. Far out in the newly forming Galaxy, the gas clouds (supergiant molecular clouds or SGMCS) in which the protoclusters are presumed to have been built would have had characteristically larger

linear sizes, to match the lower ambient pressure that was found there, in comparison to the denser conditions in the rapidly collapsing Galactic core. The timespan over which protoclusters can form scales directly with the internal free-fall time of the SGMC; thus, the cluster formation timespread will increase as the surrounding pressure drops. If the SGMC lifetime in the mid-halo region was typically  $\sim 0.5$  Gyr (see Harris & Pudritz equation 5.9 and related discussion), then it could have been  $\gtrsim 2$  Gyr in the outermost regions.

Finally, as already noted by van den Bergh (1998), the GGC which have been shown to be young are all at the low-luminosity end of the  $M_V$  distribution and are all beyond  $R_{GC} = 15$  kpc. The massive clusters beyond this Galactocentric radius do appear to be co-eval with the oldest near-halo clusters. Van den Bergh interprets this to indicate that the mass of newly-forming clusters decreased with time in the outer halo. Our present data agree with this interpretation. It will be very interesting to determine reliable ages for the remaining clusters at large  $R_{GC}$  (all relatively low-L objects) and to pursue similar studies of the low-L GGC closer to the center of the Galaxy.

Support for this work was provided by NASA to M.B., H.E.B., and R.A.B. through STScI grants GO-06106.01-94A, .02-94A, and .03-94A from the Space Telescope Science Institute, which is operated by the Association of Universities for Research in Astronomy, Incorporated, under NASA contract NAS5-26555. Financial support from the Natural Sciences and Engineering Research Council of Canada, through research grants to W.E.H., D.A.V., G.G.F., and H.B.R. is also gratefully acknowledged.

## A. [Fe/H] and $[\alpha/H]$ Determinations from the Literature

Extracting reliable relative *or* absolute age information from CMDs depends upon having accurate relative *and* absolute values for the chemical compositions of their constituent stars. In particular, the morphology of the HB is sensitive to (often unmeasurably) small differences in many parameters, among them age, [Fe/H], [CNO/Fe],  $[\alpha/\text{Fe}]$ ,  $Y$ , mass, core rotation, and so on. Thus, constraining the role played by age differences in producing a range of HB morphologies among clusters requires understanding the roles played by all other variables. A special emphasis emerges on understanding possible chemical differences which — unlike, say, interior rotation — we can, in principle, directly measure. (However, note recent papers by Rutledge, Hesser & Stetson 1997 and King *et al.* 1998, which demonstrate that there remains considerable doubt about the significance of the chemical abundances that can be inferred from existing spectroscopic observations.) Similarly, differential comparisons among remote and nearby halo objects offer a powerful tool to constrain possible age gradients as a function of Galactocentric radius, provided that we can identify near-halo clusters with compositions comparable to those of the outer-halo objects. In this section, we review information from the literature on our outer halo clusters and the comparison clusters we have chosen for them.

### A.1. General remarks

It is a risky undertaking to combine abundances from different literature studies because there is not a general agreement on the overall abundance scale. The most widely used general metallicity scale is that of Zinn & West (1984; hereinafter ZW84), which is ultimately based upon photometric, spectrophotometric, and photographic-spectrum abundance determinations from the 1970’s. Although some recent studies have called into question the zero point and scaling of absolute metallicity values from ZW84 (*e.g.*, Carretta

and Gratton 1997), it appears to provide generally reliable relative *rankings* of cluster metallicity (*e.g.*, Rutledge *et al.* 1997). Of greatest relevance to our present study, we note that in the range  $-1.0 < [\text{Fe}/\text{H}] < -1.9$ , the Zinn-West values are systematically lower by 0.23 dex than the Carretta-Gratton values. Similar trends are seen when comparing Rutledge *et al.*'s large, homogeneous survey of Ca II triplet measures to the two scales. We are fortunate that Pal 3, Pal 4 and Eridanus have all been the subject of abundance studies which allow them to be differentially compared to our two “standard” clusters M 3 and M 5 (see details below); to some extent, it is this relative ranking by metallicity that is most important for determining the range of ages among the clusters.

Because we will put high weight on  $[\text{Fe}/\text{H}]$  determinations for the outer-halo clusters that have been inferred from the lines of Ca in the near-IR, we need to be concerned not only with  $[\text{Fe}/\text{H}]$  but also with the size of the cluster-to-cluster variations in  $[\text{Ca}/\text{Fe}]$  or more generally  $[\alpha/\text{Fe}]$ . In recent years considerable observational evidence has accumulated that near-halo clusters and field stars generally display roughly constant ratios of  $\alpha$  to iron-peak elements, with the former being more abundant than the latter by several tenths of a dex for  $[\text{Fe}/\text{H}] < -1.0$ ; the  $\alpha$ -to-iron ratio approaches the solar value as  $[\text{Fe}/\text{H}]$  increases from  $-1.0$  to  $0.0$ , at least among the field stars surveyed. In a review of elemental globular cluster abundances based again on modern high-dispersion studies, Carney (1996) concludes that there is no variation of  $[\alpha/\text{Fe}]$  as a function of metallicity for 14 nearby clusters, all with  $[\text{Fe}/\text{H}] \lesssim -0.6$  to  $-0.7$ . He further summarizes the evidence for an  $\alpha$ -element enhancement relative to iron of  $[\alpha/\text{Fe}] \sim +0.28$  dex for these objects.

The great distances of the most remote clusters make fine abundance analyses challenging, and there is so far little direct evidence bearing on  $[\alpha/\text{Fe}]$  trends in the outer halo. Indeed, there are only a few such studies for clusters at intermediate  $R_{\text{GC}}$ . Brown, Wallerstein & Zucker (1997) have found that two giant stars in each of

Ruprecht 106 and Palomar 12 exhibit solar ratios of the  $\alpha$  elements (specifically, Mg, Si, Ca, and Ti), yet the clusters’ overall heavy-element abundances ( $[\text{Fe}/\text{H}] = -1.45 \pm 0.10$  and  $-1.0 \pm 0.10$ , respectively) fall in the regime where most halo objects exhibit enhanced  $\alpha$  elements. Moreover, for Rup 106 they detected an oxygen anomaly, in that its value of  $[\text{O}/\text{Fe}] = 0.0 \pm 0.13$  is about  $3\sigma$  below that normally found for stars with  $[\text{Fe}/\text{H}] \sim -1.5$ . Could such anomalies also occur in other outer-halo clusters? We have to be cautious in interpreting the latter measurement because  $[\text{O}/\text{Fe}]$  has been shown in several clusters to decrease with increasing RGB luminosity, suggesting that CNO-processed material is being dredged into the star’s atmospheres. The low  $[\text{O}/\text{Fe}]$  for the brightest Rup 106 stars may therefore not reflect the initial oxygen abundance of the stars. Based on six giants in NGC 7006 which, at  $R_{\text{GC}} = 38$  kpc, is half of the way out to the far halo, Kraft *et al.* (1998) find  $[\text{Ca}/\text{Fe}] \sim +0.2$  — consistent with the general trend of the near-halo clusters but also, at the other extreme of the error bar, possibly consistent with less  $\alpha$ -element enhancement than usual in the near halo. With its very large space velocity (Cudworth & Hanson 1993), M5 might itself be considered an outer halo denizen that shows “normal”  $[\alpha/\text{Fe}]$ .

For Population II field stars, there have been additional indications that  $[\alpha/\text{Fe}]$  may be solar or subsolar for some objects with very large space velocities and therefore large inferred apogalactic distances (*e.g.*, Carney *et al.* 1997; King 1997). It is too soon to draw any general conclusions about systematic trends in  $[\alpha/\text{Fe}]$  with  $R_{\text{GC}}$ . In what follows we must keep in mind that these remote objects may have  $[\alpha/\text{Fe}]$  ratios that are less enhanced than those of our fiducial clusters M3 and M5, and from the other calibrating clusters for the metallicity scales.



## A.2. Eridanus

Of the three outer-halo clusters, only Eridanus was included in the original ZW84 compilation; they assigned it  $[\text{Fe}/\text{H}] = -1.4$ , the same as M 5 and  $\sim 0.25$  dex more metal-rich than M 3. Armandroff & Da Costa (1991) obtained Ca II triplet spectra for two Eridanus giants along with numerous giants in six nearby well-studied clusters. Their reduced calcium equivalent widths suggested that Eridanus falls about one-third of the way from NGC 6752 ( $[\text{Fe}/\text{H}] = -1.55$ ) to NGC 1851 ( $[\text{Fe}/\text{H}] = -1.26$ ), two of their “standard” clusters. Thus from the Ca II measures alone, they derived  $-1.41 \pm 0.11$  on the ZW84 scale. (The same placement relative to NGC 6752 and NGC 1851, interpreted through the Rutledge *et al.* version of ZW84 and the Carretta-Gratton scales would be  $-1.44$  and  $-1.14$ , respectively. All three of these estimates are internally consistent to within  $\pm 0.1$  dex, given the 0.23 dex offset between ZW84 and CG97 mentioned above.) Armandroff & Da Costa combined their Ca II abundance values with two earlier estimates ( $-1.50 \pm 0.15$  by Da Costa & Armandroff (1990), derived from the position of the Eridanus giant branch in the  $(M_I, (V-I)_o)$  plane; and Da Costa’s (1985) value of  $[\text{Fe}/\text{H}] = -1.35 \pm 0.2$  determined from  $(B-V)_{o,g}$ ) to adopt a mean  $-1.42 \pm 0.08$  dex for the cluster (again on the ZW84 scale).

Earlier, Ortolani & Gratton (1989) had analyzed low-signal-to-noise, low-dispersion spectra of two Eridanus giants and four Pal 3 giants (see below). They concluded that Eridanus falls between NGC 3201 and NGC 4590 in metallicity and assigned it  $[\text{Fe}/\text{H}] = -1.6 \pm 0.3$  on their abundance scale; since ZW84 assigns metallicities of  $-1.6$  and  $-2.1$  to NGC 3201 and NGC 4590, respectively, Ortolani & Gratton’s spectra might imply  $[\text{Fe}/\text{H}] \sim -1.8$  on the ZW84 scale for Eridanus, but the error bar is large.

### A.3. Pal 3

Pal 3 and Pal 4 were included in the investigation of Armandroff, Da Costa & Zinn (1992) in which abundances were measured from the Ca II triplet. Spectra for three Pal 3 giants were measured and the reduced equivalent widths placed Pal 3 more metal-poor than M5 and similar to M13. In this study, Pal 3 was also ranked more metal-poor than Pal 4. On the ZW84 scale, Pal 3 was assigned  $[\text{Fe}/\text{H}] = -1.57 \pm 0.19$ .

Pal 3 was also part of the Ortolani & Gratton (1989) study mentioned above. From low-dispersion spectra of four giants, Pal 3 was assigned  $[\text{Fe}/\text{H}] = -1.6 \pm 0.3$  (the same as Eridanus from that study) although the star-to-star scatter was large. From their CMD for Pal 3, Ortolani & Gratton estimated  $E(B-V) = 0.03 \pm 0.02$  and  $(B-V)_{o,g} = 0.69 \pm 0.04$ , leading to  $[\text{Fe}/\text{H}] = -1.88 \pm 0.15$ . They adopted  $-1.7 \pm 0.2$  from this combination of spectral and CMD indicators.

### A.4. Pal 4

Ca II triplet measures for three giants led Armandroff *et al.* (1992) to conclude that  $[\text{Fe}/\text{H}] = -1.28 \pm 0.20$  for Pal 4 on the ZW84 scale, compared to earlier estimates from CMDs of  $[\text{Fe}/\text{H}] = -1.7$  (Christian & Heasley 1986) and  $[\text{Fe}/\text{H}] \sim -1$  (Reed & Harris 1986). They further note that their triplet metallicity determination would be  $-1.35 \pm 0.14$  were NGC 6171 excluded from their calibration. From their Figure 4, Pal 4 appears to be clearly more metal-rich than M13 and Pal 3 and comparable to or slightly more metal-rich than M5.

### A.5. Halo Cluster Metallicity Summary

The previous studies are in good general agreement in finding the Eridanus metallicity to be  $\sim -1.4$  on the ZW84 scale. To the extent that NGC 6752 is similar in  $[\text{Fe}/\text{H}]$  to M3 and M13, Eridanus appears to be more metal-rich than M3. Based primarily on the Armandroff *et al.* Ca II triplet work, we conclude that Pal 3 is closer to M3 and M13 in metallicity than it is to M5. Furthermore, by appealing to the differential studies of Armandroff *et al.* (1992) and Ortolani & Gratton (1989) we suggest that Pal 3 is the most metal-poor of our three clusters.

For purposes of comparison, our adopted  $[\text{Fe}/\text{H}]$  abundances for all five clusters, *on the ZW84 scale*, are listed in Table 6. The values for M3 and M5 are taken from the compilation of Harris (1996); each of the five is likely to be externally uncertain at the  $\pm 0.15$  dex level at least (see Paper I). Nevertheless, they indicate formally that there is no significant difference between M3 and Pal 3, or between M5 and Pal 4. On the strength of both the metallicity measurements and the CMD comparisons shown above, we believe Eridanus to be most nearly similar to M5 as well.

## REFERENCES

- Armandroff, T. E., & Da Costa, G. S. 1991, *AJ*, 101, 1329
- Armandroff, T. E., Da Costa, G. S., & Zinn, R. 1992, *AJ*, 104, 164
- Brown, J. A., Wallerstein, G., & Zucker, D. 1997, *AJ*, 114, 180
- Burbidge, E. M., & Sandage, A. 1958, *ApJ*, 127, 527
- Cardelli, J. A., Clayton, G. C., & Mathis, J. S., 1989, *ApJ*, 345, 245
- Carney, B. W. 1996, *PASP*, 108, 900
- Carney, B. W., Wright, J. S., Sneden, C., Laird, J. B., Aguilar, L. A., & Latham, D. W.  
1997, *AJ*, 114, 363
- Carretta, E., & Gratton, R. G. 1997, *A&AS*, 121, 95
- Chaboyer, B., Demarque, P., Kernan, P. J., Krauss, L. M., & Sarajedini, A. 1996*a*, *MNRAS*,  
283, 683
- Chaboyer, B., Demarque, P., & Sarajedini, A. 1996*b*, *ApJ*, 459, 558
- Chaboyer, B., Demarque, P., Kernan, P. J., and Krauss, L. M. 1998, *ApJ*, 494, 96
- Chiba, M., & Yoshii, Y. 1997, *ApJ*, 490, L73
- Christian, C. A. & Heasley, J. N. 1986, *ApJ*, 303, 216
- Cudworth, K. M., & Hanson, R. B. 1993, *AJ*, 105, 168
- Da Costa, G. S. 1985, *ApJ*, 291, 230
- Da Costa, G. S., & Armandroff, T. E. 1990, *AJ*, 100, 162

- Dorman, B. 1993, in *The Globular Cluster-Galaxy Connection*, ed. G. Smith and J. Brodie, ASP Conf. Ser., 48, 198
- Eggen, O. J., Lynden-Bell, D., & Sandage, A. 1962, *ApJ*, 136, 748 (ELS)
- Fernley, J., Barnes, T. G., Skillen, I., Hawley, S. L., Hanley, C. J., Evans, D. W., Solano, E., & Garrido, R. 1998, *A&A*, 330, 515
- Gratton, R. G., Fusi Pecci, F., Carretta, E., Clementini, G., Corsi, C. E., & Lattanzi, M. 1997, *ApJ*, 491, 749
- Gratton, R. G., & Ortolani, S. 1984, *A&AS*, 57, 177
- Greggio, L., & Renzini, A. 1983, *A&A*, 118, 217
- Harris, W. E. 1996, *AJ*, 112, 1487
- Harris, W. E., Bell, R. A., Vandenberg, D. A., Bolte, M., Stetson, P. B., Hesser, J. E., van den Bergh, S., Bond, H. E., Fahlman, G. G., & Richer, H. B. 1997, *AJ*, 114, 1030 [Paper I]
- Harris, W. E., & Pudritz, R. E. 1994, *ApJ*, 429, 177
- Hendry, M. A. 1997, *Observatory*, 117, 329
- Hesser, J. E., Shawl, S. J., & Meyer, J. E. 1986, *PASP*, 98, 403
- Holtzman, J. A., Burrows, C. J., Casertano, S., Hester, J. J., Trauger, J. T., Watson, A. M., & Worthey, G. 1995, *PASP*, 107, 1065
- Huchra, J. P., Brodie, J. P., & Kent, S. M. 1991, *ApJ*, 370, 495
- Itoh, N., Hayashi, H., Nishikawa, A., & Kohyama, Y. 1996, *ApJS*, 102, 411
- Johnson, J. A., & Bolte, M., 1998, *AJ*, 115, 693

King, J. R. 1994, AJ, 107, 350

King, J. R. 1997, AJ, 113, 2302

King, J. R., Stephens, A., Boesgaard, A. M., & Deliyannis, C. P. 1998, AJ, 115, 666

Kinman, T. D. 1959, MNRAS, 119, 538

Kraft, R. P., Sneden, C., Smith, G. H., Shetrone, M. D., & Fulbright, J. 1998, AJ, in press

Landolt, A. U. 1992, AJ, 104, 340

Lee, Y.-W. 1992, AJ, 104, 1780

Lee, Y.-W., Demarque, P., & Zinn, R. 1994, ApJ, 423, 248 (LDZ)

Majewski, S. 1994, ApJ, 431, L17

Minniti, D. 1995, AJ, 109, 1663

Ortolani, S., & Gratton, R. G. 1989, A&AS, 79, 155

Pont, F., Mayor, M., Turon, C., & Vandenberg, D. A. 1998, A&A, 329, 87

Reed, B. C., & Harris, W. E., 1986, AJ, 91, 81

Rodgers, A. W., & Paltoglou, G. 1984, ApJ, 283, L5

Rutledge, G. A., Hesser, J. E., & Stetson, P. B. 1997, PASP, 109, 907

Sandage, A. 1990, JRASC, 84, 70

Sandquist, E. L., Bolte, M., Stetson, P. B., & Hesser, J. E. 1996, ApJ, 470, 910

Sarajedini, A. 1997, AJ, 113, 682

Sarajedini, A., Chaboyer, B., & Demarque, P. 1997, PASP, 109, 1321

- Searle, L., & Zinn, R. 1978, *ApJ*, 225, 357 (SZ)
- Smecker-Hane, T. A., & Wyse, R. F. G. 1992, *AJ*, 103, 1621
- Stetson, P. B. 1987, *PASP*, 99, 191
- Stetson, P. B. 1990, in *CCDs in Astronomy. II. New Methods and Applications of CCD Technology*, ed. A. G. D. Philip, D. S. Hayes, & S. J. Adelman (Schenectady: L. Davis Press), 71
- Stetson, P. B. 1993, in *IAU Coll. 136, Stellar Photometry — Current Techniques and Future Developments*, ed. C. J. Butler & I. Elliot (Cambridge: Cambridge Univ. Press), 291
- Stetson, P. B. 1994, *PASP*, 106, 250
- Stetson, P. B., Vandenberg, D. A., & Bolte, M. 1996, *PASP*, 108, 560
- Sweigart, A. V. 1997, *ApJ*, 474, L23
- Vandenberg, D. A., Bolte, M., & Stetson, P. B. 1990, *AJ*, 100, 445 (VBS)
- van den Bergh, S. 1993, *ApJ*, 411, 178
- Whitmore, B., & Heyer, I. 1997, *Instrument Science Report WFPC2 97-08* (Baltimore: STScI)
- Zinn, R. 1985, *ApJ*, 293, 424
- Zinn, R. 1993, in *The Globular Cluster-Galaxy Connection*, ed. G. Smith and J. Brodie, *ASP Conf. Ser.*, 48, 38
- Zinn, R. 1996, in *Formation of the Galactic Halo ... Inside and Out*, ed. H. Morrison and A. Sarajedini, *ASP Conf. Ser.*, 92, 211
- Zinn, R., & West, M. J. 1984, *ApJS*, 55, 45





Fig. 1.— Color-magnitude diagram for the outer-halo globular cluster Pal 3, derived from our WFPC2 photometry with the *HST*. Only stars with photometric standard errors  $\sigma(V-I) < 0.10$  mag have been plotted, and data from all four CCD fields have been combined. The circled cross at the blue end of the HB represents the mean magnitude and color of 7 RR Lyrae stars in the cluster.

Fig. 2.— Color-magnitude diagram for Pal 4, as in Fig. 1.

Fig. 3.— Color-magnitude diagram for Eridanus, as in Fig. 1.

Fig. 4.— Ground-based ( $V, V-I$ ) color-magnitude diagram for the nearby globular cluster M3. Only stars with photometric standard errors  $\sigma(V-I) < 0.10$  mag have been plotted.

Fig. 5.— Ground-based ( $V, V-I$ ) color-magnitude diagram for the nearby globular cluster M5, as in Fig. 4.

Fig. 6.— Light-curve fragments for seven candidate RR Lyrae variables in the outer-halo globular cluster Pal 3, based upon our *HST* observations. Open squares represent instantaneous  $I$ -band magnitudes, and closed circles represent  $V$ -band magnitudes.

Fig. 7.— The open squares are our fiducial points for the CMD of Pal 3, as determined by mean colors after three iterations of  $\sigma$ -clipping in bins of height 0.2 mag in  $V$ . The solid curve is a robust maximum-likelihood fit of which isochrone that best matches the observed CMD from among a wide variety of isochrones that were tried. For the HB level and brighter, the individual HB and RGB stars are plotted (crosses).

Fig. 8.— Fiducial points and isochrone fit for the CMD of Pal 4, with symbols as described in Figure 7.

Fig. 9.— Fiducial points and isochrone fit for the CMD of Eridanus, with symbols as described in Figure 7.

Fig. 10.— Fiducial points and isochrone fit for the CMD of M 3, with symbols as described in Figure 7.

Fig. 11.— Fiducial points and isochrone fit for the CMD of M 5, with symbols as described in Figure 7.

Fig. 12.— Theoretical isochrones for chemical-abundance ratios  $[\text{Fe}/\text{H}] = -1.41$  and  $[\alpha/\text{Fe}] = +0.3$ , and ages of 8 to 16 Gyr in steps of 2 Gyr, illustrating the predicted dependence of CMD morphology on age, as described in the text.

Fig. 13.— Theoretical isochrones for chemical-abundance ratios  $[\text{Fe}/\text{H}] = -1.14, -1.41,$  and  $-1.61$ ;  $[\alpha/\text{Fe}] = +0.3$ ; and an age of 12 Gyr, illustrating the predicted dependence of CMD morphology on relative iron abundance. The isochrones have been shifted horizontally and vertically as in Fig. 12.

Fig. 14.— Theoretical isochrones for  $[\text{Fe}/\text{H}] = -1.41$ ;  $[\alpha/\text{Fe}] = 0.0, +0.3,$  and  $+0.6$ ; and an age of 12 Gyr, illustrating the predicted dependence of CMD morphology on relative  $\alpha$ -element abundance. The isochrones have been shifted horizontally and vertically as in Fig. 12.

Fig. 15.— Fiducial points for the three outer-halo clusters (Pal 3, Pal 4, and Eridanus), dereddened according to the values listed in Table 6, and shifted vertically to match their red HBs (the short horizontal line at  $M_V = 0.70$  represents the RHB level of each cluster). The distance scale for  $M_V(\text{HB})$  has been chosen arbitrarily for comparison purposes. Note that the mean points for Pal 4 and Eridanus are essentially indistinguishable; the giant branch of Pal 3 lies  $\simeq 0.02$  magnitude to the blue of the GBs of the other two clusters.

Fig. 16.— The mean points for Pal 3, Pal 4, and Eridanus have been re-registered as prescribed by VandenBerg, Bolte, & Stetson (1990): the CMDs have been shifted horizontally

so that the MSTO colors coincide (vertical line), and vertically so that the point on the main sequence 0.05 mag redder than the MSTO coincides (horizontal line). The horizontal shifts were taken from the isochrone fits (Table 3), which produce estimated turnoff colors systematically 0.007 mag bluer than  $\sigma$ -clipped normal points given in Table 2; thus there appears to be a slight offset of the turnoff points from  $\Delta(V-I) \equiv 0.00$ . This offset is nearly identical for the three clusters, so no material harm is done to the differential analysis. For a given composition, an age difference appears as an offset in the RGB color. Pal 4 and Eridanus appear to be indistinguishable in age, while Pal 3 may be slightly older. If the clusters do not have identical abundances, the interpretation of this diagram becomes more complex, as described in the text.

Fig. 17.— The data for Pal 3, Pal 4, and Eridanus have been registered as in Fig. 16, except in this case the stars have been plotted individually. The curve-sided box represents the region where the relative displacements of the three giant branches were determined, as listed in Table 4. Only stars with  $\sigma(V-I) < 0.05$  mag have been plotted. Symbol types are as in Fig. 16.

Fig. 18.— Stars in the region of the red HB have been plotted for (from top to bottom) Pal 3, Pal 4, Eridanus, M3, and M5. The photometry has been dereddened according to the color excesses in Table 6, with the assumption that  $E(V-I) = 1.3E(B-V)$ . The solid curves represent our eyeball fits of theoretical ZAHB loci to the lower envelope of the horizontal-branch stars for each cluster.

Fig. 19.— Horizontal-branch region of the CMD of M5 based upon the  $V, I$  data of Sandquist *et al.* (1996), after correcting for minor zero-point shifts in the photometry as described in the text. The solid curve is the same ZAHB locus as in the bottom panel of Fig. 18. Here,  $(m-M)_V$  denotes the vertical shift required to register theoretical luminosities  $M_V$  with observed  $V$ -band magnitudes; due to uncertainties in the modelling, this may not accurately

represent the actual geometric distance of the cluster.

Fig. 20.— The relationship between the giant-branch-to-turnoff color difference (abscissa) and the horizontal-branch-to-turnoff magnitude difference (ordinate), according to the present set of isochrones. The solid curve represents the predicted track followed by a globular cluster with  $[\text{Fe}/\text{H}] = -1.41$  and  $[\alpha/\text{Fe}] = +0.3$  as it ages from 8 Gyr (top right) to 18 Gyr (bottom left) according to the present set of theoretical models. The absolute placement of the curve and tick marks are uncertain due to incomplete knowledge of the physics of stellar interiors, but the size of the intervals, representing age differences of 2 Gyr, or 15–20%, should be correct in a relative sense. The arrow represents the amount by which the models would be shifted for an iron or  $\alpha$ -element abundance 0.2 dex larger. The positions in this diagram currently occupied by the outer-halo globular clusters are represented by open symbols: triangle (Pal 3), square (Pal 4), and circle (Eridanus). The near-halo clusters are represented by closed symbols: triangle (M 3) and pentagon (M 5). The cross in the lower right represents our estimate of the random observational errors ( $\pm 1\sigma$ ) in the two coordinates.

Table 1. Notional Periods for Candidate RR Lyrae Variables

Star ID	extremum	HJD– 2 449 800	extremum	HJD– 2 449 800	$\Delta t$	$n \times P?$
1-233	<i>I</i> minimum	20.68	<i>V</i> minimum	$\gtrsim 22.49$	1.81	$3 \times 0.60$
1-299	<i>I</i> minimum	20.82	<i>V</i> minimum	$\lesssim 22.01$	1.19	$2 \times 0.60$
1-404	<i>I</i> minimum	20.62	<i>V</i> minimum	22.42	1.80	$3 \times 0.60$
2-198	<i>I</i> minimum	20.61	<i>V</i> minimum	22.35	1.74	$3 \times 0.58$
2-368	<i>I</i> maximum	20.55	<i>V</i> maximum	22.36	1.81	$3 \times 0.60$
2-614	<i>I</i> minimum	20.82	<i>V</i> minimum	$\lesssim 22.01$	1.19	$2 \times 0.60$
3-269	<i>I</i> maximum	20.61	<i>V</i> maximum	22.42	1.81	$3 \times 0.60$

Table 2. Normal Points for Program Clusters

$V$	$V-I$	$n_1$	$n_2$	$n_3$
a. Palomar 3				
$20.884 \pm 0.034$	$0.978 \pm 0.024$	3	3	3
$21.526 \pm 0.045$	$0.908 \pm 0.014$	3	3	3
$21.742 \pm 0.019$	$0.919 \pm 0.004$	7	7	7
$21.936 \pm 0.026$	$0.887 \pm 0.012$	3	3	3
$22.119 \pm 0.016$	$0.890 \pm 0.005$	10	9	8
$22.295 \pm 0.030$	$0.885 \pm 0.007$	6	6	6
$22.525 \pm 0.023$	$0.847 \pm 0.019$	7	7	7
$22.690 \pm 0.023$	$0.862 \pm 0.008$	4	4	4
$22.927 \pm 0.022$	$0.807 \pm 0.014$	10	9	9
$23.099 \pm 0.011$	$0.777 \pm 0.008$	36	34	33
$23.299 \pm 0.010$	$0.676 \pm 0.005$	34	31	30
$23.508 \pm 0.010$	$0.629 \pm 0.003$	47	44	40
$23.690 \pm 0.010$	$0.622 \pm 0.002$	48	44	43
$23.919 \pm 0.007$	$0.630 \pm 0.003$	70	67	64
$24.103 \pm 0.006$	$0.627 \pm 0.003$	87	85	81
$24.295 \pm 0.007$	$0.639 \pm 0.002$	99	93	89
$24.501 \pm 0.005$	$0.652 \pm 0.002$	122	115	109
$24.705 \pm 0.006$	$0.674 \pm 0.003$	117	111	107
$24.908 \pm 0.006$	$0.701 \pm 0.004$	117	114	111
$25.093 \pm 0.005$	$0.720 \pm 0.004$	142	138	132
$25.304 \pm 0.005$	$0.738 \pm 0.004$	153	147	139
$25.501 \pm 0.005$	$0.764 \pm 0.003$	180	170	162
$25.698 \pm 0.005$	$0.800 \pm 0.004$	204	193	183
$25.894 \pm 0.004$	$0.830 \pm 0.004$	180	172	164
$26.100 \pm 0.004$	$0.867 \pm 0.005$	184	177	171
$26.299 \pm 0.005$	$0.913 \pm 0.006$	167	157	147
$26.502 \pm 0.005$	$0.955 \pm 0.006$	163	155	149

Table 2—Continued

$V$	$V-I$	$n_1$	$n_2$	$n_3$
$26.686 \pm 0.005$	$0.997 \pm 0.007$	131	126	119
$26.893 \pm 0.005$	$1.048 \pm 0.009$	96	91	85
$27.091 \pm 0.011$	$1.037 \pm 0.018$	34	33	33
$27.257 \pm 0.016$	$1.093 \pm 0.014$	17	16	15
$27.493 \pm 0.062$	$1.157 \pm 0.013$	3	3	3
b. Palomar 4				
$20.119 \pm 0.064$	$1.082 \pm 0.008$	3	3	3
$20.504 \pm 0.025$	$1.025 \pm 0.007$	6	6	6
$20.663 \pm 0.022$	$1.007 \pm 0.010$	5	5	5
$21.127 \pm 0.023$	$0.967 \pm 0.005$	4	4	4
$21.305 \pm 0.043$	$0.968 \pm 0.018$	4	4	4
$21.492 \pm 0.031$	$0.950 \pm 0.005$	4	4	4
$22.095 \pm 0.019$	$0.907 \pm 0.004$	7	7	7
$22.327 \pm 0.029$	$0.892 \pm 0.002$	6	6	6
$22.441 \pm 0.021$	$0.893 \pm 0.000$	3	3	3
$22.680 \pm 0.020$	$0.877 \pm 0.005$	12	11	11
$22.914 \pm 0.020$	$0.885 \pm 0.009$	12	11	10
$23.090 \pm 0.015$	$0.837 \pm 0.008$	16	15	14
$23.331 \pm 0.011$	$0.817 \pm 0.006$	22	20	19
$23.508 \pm 0.006$	$0.724 \pm 0.006$	67	66	66
$23.714 \pm 0.007$	$0.644 \pm 0.002$	61	58	55
$23.901 \pm 0.007$	$0.617 \pm 0.003$	70	67	66
$24.098 \pm 0.006$	$0.621 \pm 0.002$	96	93	89
$24.299 \pm 0.006$	$0.620 \pm 0.003$	109	103	99
$24.499 \pm 0.005$	$0.632 \pm 0.003$	132	129	124
$24.699 \pm 0.005$	$0.645 \pm 0.002$	159	151	143
$24.908 \pm 0.004$	$0.665 \pm 0.003$	167	160	153
$25.095 \pm 0.005$	$0.682 \pm 0.003$	165	161	151

Table 2—Continued

$V$	$V-I$	$n_1$	$n_2$	$n_3$
$25.300 \pm 0.004$	$0.706 \pm 0.002$	224	209	195
$25.500 \pm 0.004$	$0.726 \pm 0.003$	229	215	206
$25.698 \pm 0.004$	$0.753 \pm 0.003$	227	212	201
$25.908 \pm 0.004$	$0.787 \pm 0.004$	205	190	182
$26.099 \pm 0.004$	$0.826 \pm 0.005$	195	184	172
$26.288 \pm 0.004$	$0.845 \pm 0.006$	176	166	159
$26.502 \pm 0.004$	$0.893 \pm 0.008$	159	151	144
$26.698 \pm 0.005$	$0.956 \pm 0.009$	137	132	126
c. Eridanus				
$20.887 \pm 0.026$	$1.003 \pm 0.023$	4	4	4
$21.339 \pm 0.022$	$0.935 \pm 0.013$	3	3	3
$21.467 \pm 0.021$	$0.923 \pm 0.014$	6	6	6
$21.701 \pm 0.024$	$0.913 \pm 0.006$	8	7	7
$21.882 \pm 0.039$	$0.876 \pm 0.016$	6	6	6
$22.130 \pm 0.023$	$0.899 \pm 0.012$	4	4	4
$22.284 \pm 0.034$	$0.878 \pm 0.010$	5	5	5
$22.524 \pm 0.018$	$0.857 \pm 0.006$	9	8	8
$22.711 \pm 0.018$	$0.842 \pm 0.008$	7	6	6
$22.886 \pm 0.022$	$0.818 \pm 0.008$	12	11	11
$23.102 \pm 0.010$	$0.698 \pm 0.007$	35	34	34
$23.303 \pm 0.009$	$0.638 \pm 0.004$	40	40	40
$23.485 \pm 0.007$	$0.624 \pm 0.004$	54	53	52
$23.710 \pm 0.007$	$0.615 \pm 0.004$	59	57	54
$23.919 \pm 0.007$	$0.621 \pm 0.004$	66	64	60
$24.094 \pm 0.007$	$0.636 \pm 0.004$	82	79	76
$24.299 \pm 0.006$	$0.646 \pm 0.004$	83	80	77
$24.496 \pm 0.006$	$0.664 \pm 0.003$	125	119	111
$24.690 \pm 0.006$	$0.682 \pm 0.004$	104	97	93



Table 2—Continued

$V$	$V-I$	$n_1$	$n_2$	$n_3$
$24.888 \pm 0.006$	$0.711 \pm 0.003$	113	107	101
$25.092 \pm 0.006$	$0.731 \pm 0.005$	112	105	98
$25.307 \pm 0.005$	$0.747 \pm 0.006$	113	110	107
$25.502 \pm 0.005$	$0.790 \pm 0.005$	130	123	117
$25.701 \pm 0.005$	$0.814 \pm 0.006$	113	109	104
$25.899 \pm 0.005$	$0.841 \pm 0.007$	141	134	129
$26.108 \pm 0.005$	$0.906 \pm 0.007$	115	109	104
$26.300 \pm 0.006$	$0.942 \pm 0.009$	127	121	118
$26.502 \pm 0.006$	$0.998 \pm 0.009$	115	111	107
$26.706 \pm 0.007$	$1.035 \pm 0.011$	91	86	84
$26.891 \pm 0.006$	$1.048 \pm 0.010$	85	81	80
$27.092 \pm 0.007$	$1.043 \pm 0.014$	65	62	59
$27.274 \pm 0.014$	$1.093 \pm 0.025$	20	19	18
$27.472 \pm 0.027$	$1.109 \pm 0.021$	7	7	7
d. M3				
$15.031 \pm 0.018$	$0.993 \pm 0.004$	3	3	3
$16.343 \pm 0.014$	$0.882 \pm 0.005$	6	6	6
$16.433 \pm 0.017$	$0.881 \pm 0.005$	3	3	3
$16.660 \pm 0.004$	$0.874 \pm 0.017$	4	4	4
$16.931 \pm 0.020$	$0.846 \pm 0.008$	4	4	4
$17.736 \pm 0.014$	$0.810 \pm 0.007$	3	3	3
$17.931 \pm 0.010$	$0.812 \pm 0.007$	5	5	5
$18.034 \pm 0.009$	$0.799 \pm 0.007$	8	8	8
$18.235 \pm 0.007$	$0.780 \pm 0.006$	8	7	7
$18.363 \pm 0.007$	$0.743 \pm 0.008$	19	18	18
$18.455 \pm 0.006$	$0.680 \pm 0.009$	20	20	20
$18.552 \pm 0.007$	$0.647 \pm 0.005$	23	22	21
$18.655 \pm 0.009$	$0.608 \pm 0.011$	14	14	14

Table 2—Continued

$V$	$V-I$	$n_1$	$n_2$	$n_3$
$18.744 \pm 0.005$	$0.610 \pm 0.003$	34	32	30
$18.865 \pm 0.005$	$0.583 \pm 0.003$	30	29	29
$18.953 \pm 0.006$	$0.585 \pm 0.002$	41	39	37
$19.048 \pm 0.004$	$0.581 \pm 0.002$	44	41	40
$19.151 \pm 0.005$	$0.584 \pm 0.002$	53	50	49
$19.250 \pm 0.003$	$0.581 \pm 0.002$	59	54	51
$19.346 \pm 0.004$	$0.581 \pm 0.002$	53	50	45
$19.447 \pm 0.004$	$0.589 \pm 0.002$	53	49	49
$19.545 \pm 0.004$	$0.590 \pm 0.002$	60	57	54
$19.656 \pm 0.004$	$0.606 \pm 0.003$	56	52	50
$19.752 \pm 0.004$	$0.609 \pm 0.003$	55	53	49
$19.848 \pm 0.003$	$0.614 \pm 0.002$	66	61	56
$19.954 \pm 0.004$	$0.628 \pm 0.003$	67	65	61
$20.057 \pm 0.004$	$0.638 \pm 0.002$	73	69	65
$20.149 \pm 0.004$	$0.646 \pm 0.003$	74	69	63
$20.247 \pm 0.003$	$0.659 \pm 0.002$	80	75	72
$20.349 \pm 0.003$	$0.672 \pm 0.003$	78	77	74
$20.454 \pm 0.003$	$0.687 \pm 0.002$	82	75	70
$20.546 \pm 0.004$	$0.702 \pm 0.003$	97	90	86
$20.646 \pm 0.003$	$0.715 \pm 0.003$	93	91	84
$20.754 \pm 0.004$	$0.734 \pm 0.004$	89	88	82
$20.850 \pm 0.004$	$0.749 \pm 0.003$	64	59	55
$20.950 \pm 0.003$	$0.760 \pm 0.003$	95	90	84
$21.053 \pm 0.004$	$0.777 \pm 0.003$	85	81	77
$21.149 \pm 0.003$	$0.796 \pm 0.003$	75	72	67
$21.247 \pm 0.003$	$0.813 \pm 0.005$	67	65	61
$21.352 \pm 0.004$	$0.829 \pm 0.003$	58	55	53
$21.444 \pm 0.004$	$0.847 \pm 0.004$	61	56	52

Table 2—Continued

$V$	$V-I$	$n_1$	$n_2$	$n_3$
$21.552 \pm 0.005$	$0.875 \pm 0.003$	49	46	44
$21.649 \pm 0.004$	$0.895 \pm 0.004$	49	45	42
$21.753 \pm 0.005$	$0.914 \pm 0.004$	53	50	47
$21.849 \pm 0.004$	$0.941 \pm 0.005$	49	47	43
$21.937 \pm 0.005$	$0.966 \pm 0.006$	44	41	39
$22.058 \pm 0.004$	$0.987 \pm 0.006$	49	47	43
$22.142 \pm 0.005$	$1.009 \pm 0.005$	41	38	36
$22.254 \pm 0.005$	$1.033 \pm 0.006$	35	32	31
$22.343 \pm 0.005$	$1.055 \pm 0.005$	39	36	34
$22.450 \pm 0.004$	$1.078 \pm 0.004$	46	42	41
$22.550 \pm 0.005$	$1.113 \pm 0.008$	31	29	27
$22.637 \pm 0.008$	$1.183 \pm 0.015$	17	16	16
$22.758 \pm 0.009$	$1.166 \pm 0.021$	10	10	10
$22.830 \pm 0.009$	$1.178 \pm 0.019$	6	6	6
e. M5				
$14.954 \pm 0.021$	$1.004 \pm 0.012$	3	3	3
$15.039 \pm 0.036$	$0.996 \pm 0.003$	3	3	3
$15.570 \pm 0.016$	$0.948 \pm 0.013$	4	4	4
$15.645 \pm 0.032$	$0.945 \pm 0.009$	3	3	3
$15.854 \pm 0.021$	$0.930 \pm 0.011$	4	4	4
$15.965 \pm 0.016$	$0.928 \pm 0.011$	4	4	4
$16.432 \pm 0.013$	$0.894 \pm 0.012$	5	5	5
$16.557 \pm 0.017$	$0.890 \pm 0.006$	5	5	5
$16.678 \pm 0.007$	$0.888 \pm 0.005$	4	4	4
$16.758 \pm 0.005$	$0.873 \pm 0.005$	5	5	5
$16.948 \pm 0.009$	$0.877 \pm 0.008$	8	8	8
$17.042 \pm 0.013$	$0.869 \pm 0.010$	7	7	7
$17.156 \pm 0.005$	$0.865 \pm 0.004$	12	12	12

Table 2—Continued

$V$	$V-I$	$n_1$	$n_2$	$n_3$
$17.283 \pm 0.005$	$0.834 \pm 0.009$	3	3	3
$17.361 \pm 0.015$	$0.848 \pm 0.011$	6	6	6
$17.432 \pm 0.011$	$0.858 \pm 0.008$	5	5	5
$17.558 \pm 0.010$	$0.828 \pm 0.007$	10	10	10
$17.653 \pm 0.009$	$0.830 \pm 0.007$	11	11	11
$17.751 \pm 0.011$	$0.809 \pm 0.013$	8	7	7
$17.856 \pm 0.007$	$0.767 \pm 0.006$	26	26	26
$17.952 \pm 0.006$	$0.717 \pm 0.005$	34	31	30
$18.050 \pm 0.006$	$0.674 \pm 0.003$	27	25	23
$18.148 \pm 0.007$	$0.641 \pm 0.002$	30	27	26
$18.248 \pm 0.006$	$0.630 \pm 0.003$	36	32	31
$18.361 \pm 0.004$	$0.624 \pm 0.003$	38	37	36
$18.453 \pm 0.005$	$0.631 \pm 0.003$	46	45	42
$18.537 \pm 0.006$	$0.624 \pm 0.005$	26	25	24
$18.645 \pm 0.004$	$0.627 \pm 0.002$	58	55	53
$18.749 \pm 0.004$	$0.631 \pm 0.003$	49	46	45
$18.847 \pm 0.004$	$0.633 \pm 0.003$	50	49	46
$18.958 \pm 0.005$	$0.641 \pm 0.003$	48	46	44
$19.055 \pm 0.003$	$0.648 \pm 0.003$	50	49	48
$19.158 \pm 0.005$	$0.650 \pm 0.002$	49	48	45
$19.250 \pm 0.004$	$0.661 \pm 0.003$	56	55	53
$19.352 \pm 0.003$	$0.668 \pm 0.003$	74	70	69
$19.450 \pm 0.004$	$0.675 \pm 0.002$	60	58	54
$19.551 \pm 0.004$	$0.688 \pm 0.002$	89	86	82
$19.658 \pm 0.004$	$0.698 \pm 0.003$	50	48	47
$19.751 \pm 0.004$	$0.709 \pm 0.003$	69	67	64
$19.851 \pm 0.004$	$0.719 \pm 0.003$	65	62	61
$19.955 \pm 0.004$	$0.742 \pm 0.003$	60	56	54

Table 2—Continued

$V$	$V-I$	$n_1$	$n_2$	$n_3$
$20.049 \pm 0.004$	$0.746 \pm 0.003$	85	81	77
$20.154 \pm 0.004$	$0.765 \pm 0.003$	65	63	60
$20.255 \pm 0.004$	$0.780 \pm 0.003$	63	62	60
$20.345 \pm 0.004$	$0.783 \pm 0.004$	58	56	52
$20.448 \pm 0.003$	$0.809 \pm 0.003$	66	63	62
$20.545 \pm 0.004$	$0.829 \pm 0.004$	62	59	57
$20.649 \pm 0.004$	$0.840 \pm 0.003$	64	60	58
$20.744 \pm 0.004$	$0.857 \pm 0.005$	60	57	54
$20.852 \pm 0.002$	$0.875 \pm 0.003$	68	65	63
$20.946 \pm 0.004$	$0.898 \pm 0.005$	46	45	44
$21.044 \pm 0.005$	$0.916 \pm 0.004$	54	51	48
$21.140 \pm 0.004$	$0.930 \pm 0.004$	47	44	42
$21.258 \pm 0.005$	$0.969 \pm 0.005$	42	40	40
$21.356 \pm 0.005$	$0.985 \pm 0.005$	37	35	32
$21.441 \pm 0.004$	$1.002 \pm 0.004$	44	42	40
$21.552 \pm 0.005$	$1.036 \pm 0.006$	36	34	34
$21.660 \pm 0.005$	$1.058 \pm 0.006$	32	30	29
$21.746 \pm 0.006$	$1.073 \pm 0.010$	19	18	17
$21.858 \pm 0.007$	$1.095 \pm 0.009$	23	22	21
$21.958 \pm 0.006$	$1.162 \pm 0.007$	27	25	24
$22.058 \pm 0.007$	$1.168 \pm 0.010$	17	17	17
$22.134 \pm 0.007$	$1.186 \pm 0.013$	19	18	17
$22.251 \pm 0.011$	$1.275 \pm 0.017$	11	11	11
$22.346 \pm 0.015$	$1.244 \pm 0.043$	3	3	3
$22.537 \pm 0.023$	$1.350 \pm 0.024$	3	3	3

Table 3. Turnoff Locations for Program Clusters

Cluster	$V_{MSTO}$	$(V-I)_{MSTO}$	$V_{+0.10}^-$	$V_{+0.05}^-$	$V_{+0.05}^+$	$V_{+0.10}^+$
Palomar 3	23.83	0.614	23.22	23.35	24.63	25.09
Palomar 4	24.12	0.614	23.52	23.64	24.93	25.38
Eridanus	23.70	0.610	23.09	23.21	24.50	24.95
M 3	19.16	0.578	18.53	18.67	19.97	20.40
M 5	18.56	0.614	17.95	18.09	19.37	19.84

Table 4. Giant-Branch Offsets for Program Clusters

Cluster	mean offset	median offset	standard deviation	N	median $\sigma(V-I)$
Palomar 3	-0.0035	-0.001	0.021	45	0.013
Palomar 4	-0.0037	-0.003	0.012	51	0.011
Eridanus	+0.0078	+0.009	0.020	46	0.014

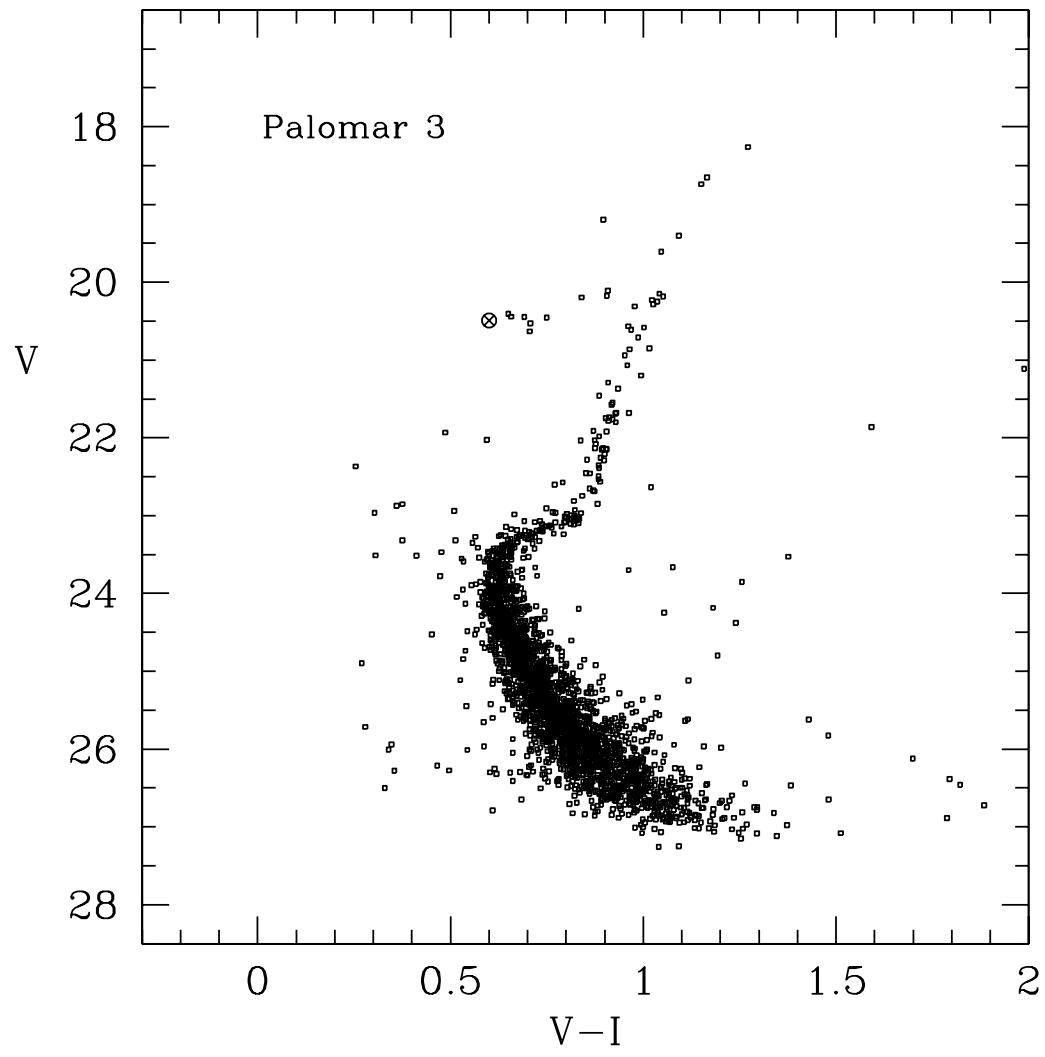
Table 5. Giant-Branch Offsets for Program Clusters

Cluster	mean offset	median offset	standard deviation	N	median $\sigma(V-I)$
Palomar 3	+0.0096	+0.015	0.020	44	0.013
Palomar 4	+0.0123	+0.012	0.010	50	0.011
Eridanus	+0.0205	+0.026	0.022	45	0.014
M 3	-0.0139	-0.015	0.014	46	0.005
M 5	-0.0073	-0.006	0.019	85	0.010

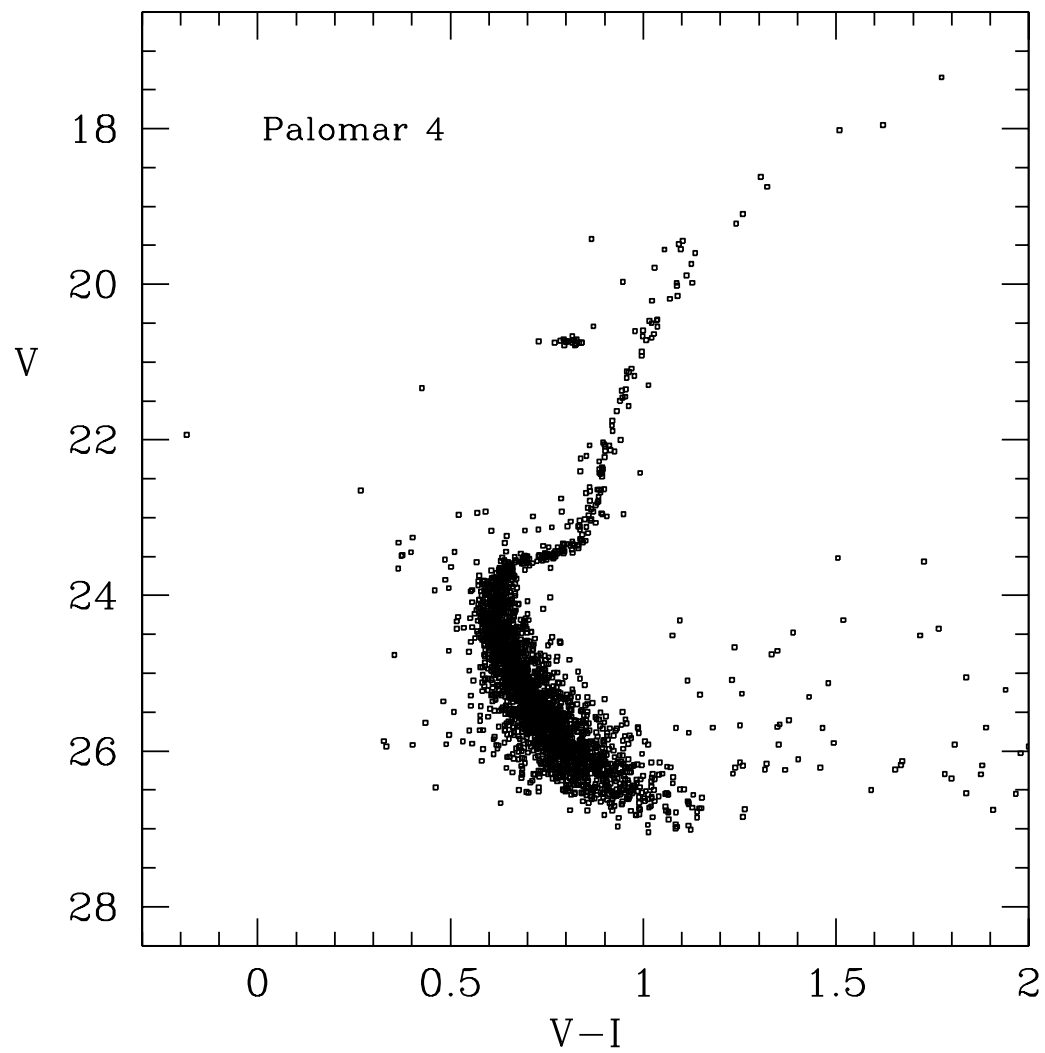


Table 6. Fiducial Parameters for Program Clusters

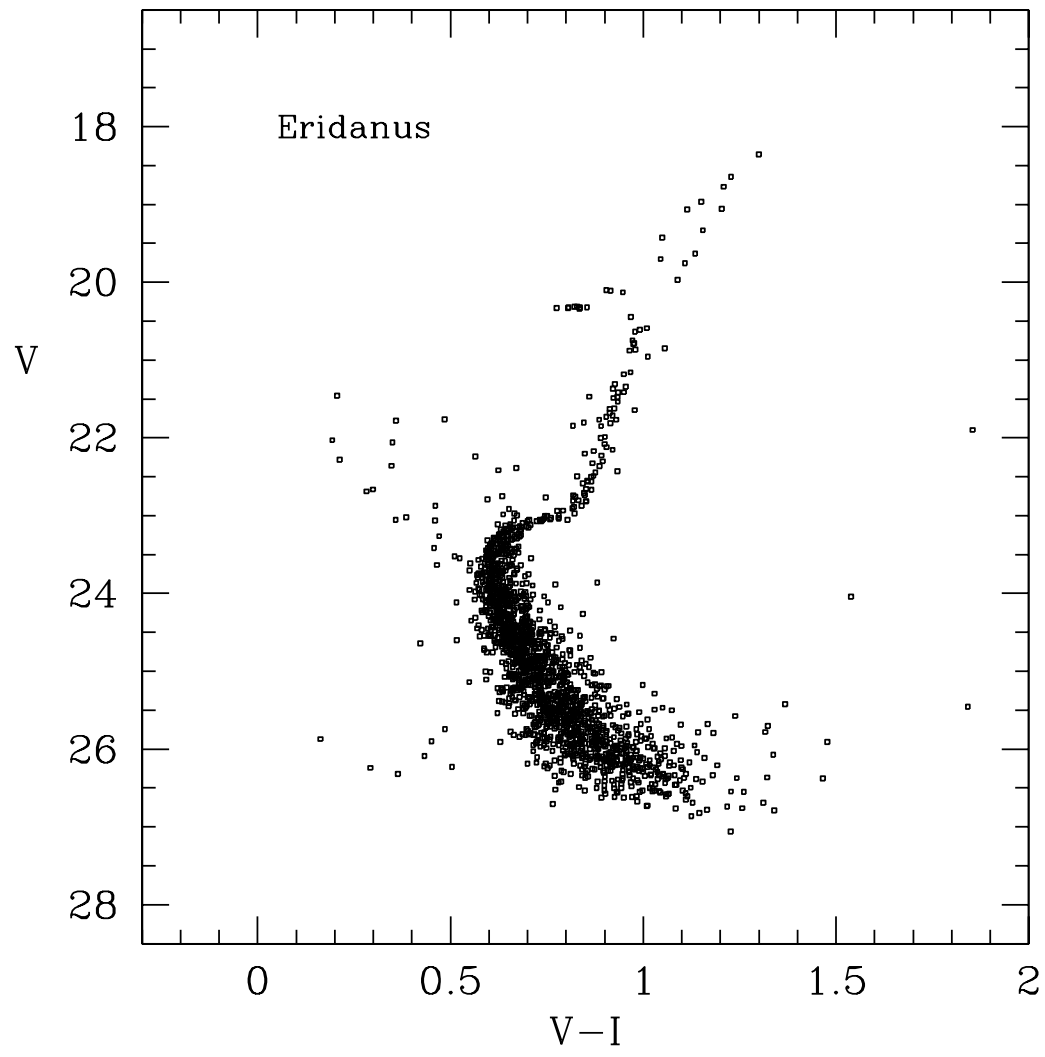
Cluster	[Fe/H]	$E(B-V)$	$(V-I)_{\circ,TO}$	$V_{HB}$	$V_{MSTO}$	$\Delta V$
Palomar 3	−1.57	0.03	0.579	20.51	23.83	3.32
Palomar 4	−1.28	0.01	0.595	20.80	24.12	3.32
Eridanus	−1.42	0.02	0.590	20.42	23.70	3.28
M 3	−1.57	0.01	0.578	15.68	19.14	3.46
M 5	−1.29	0.03	0.579	15.15	18.59	3.44



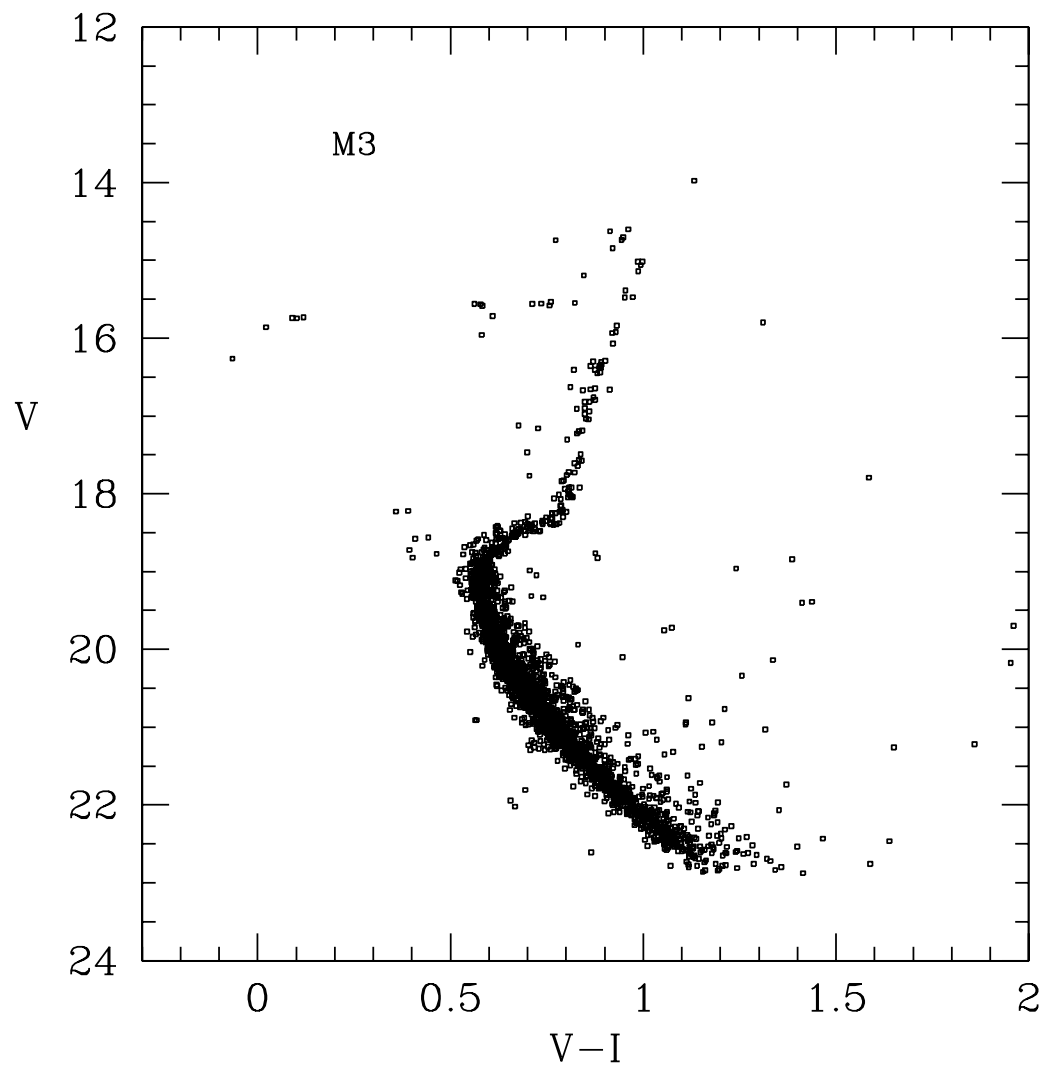
Stetson *et al.* --- Fig. 1



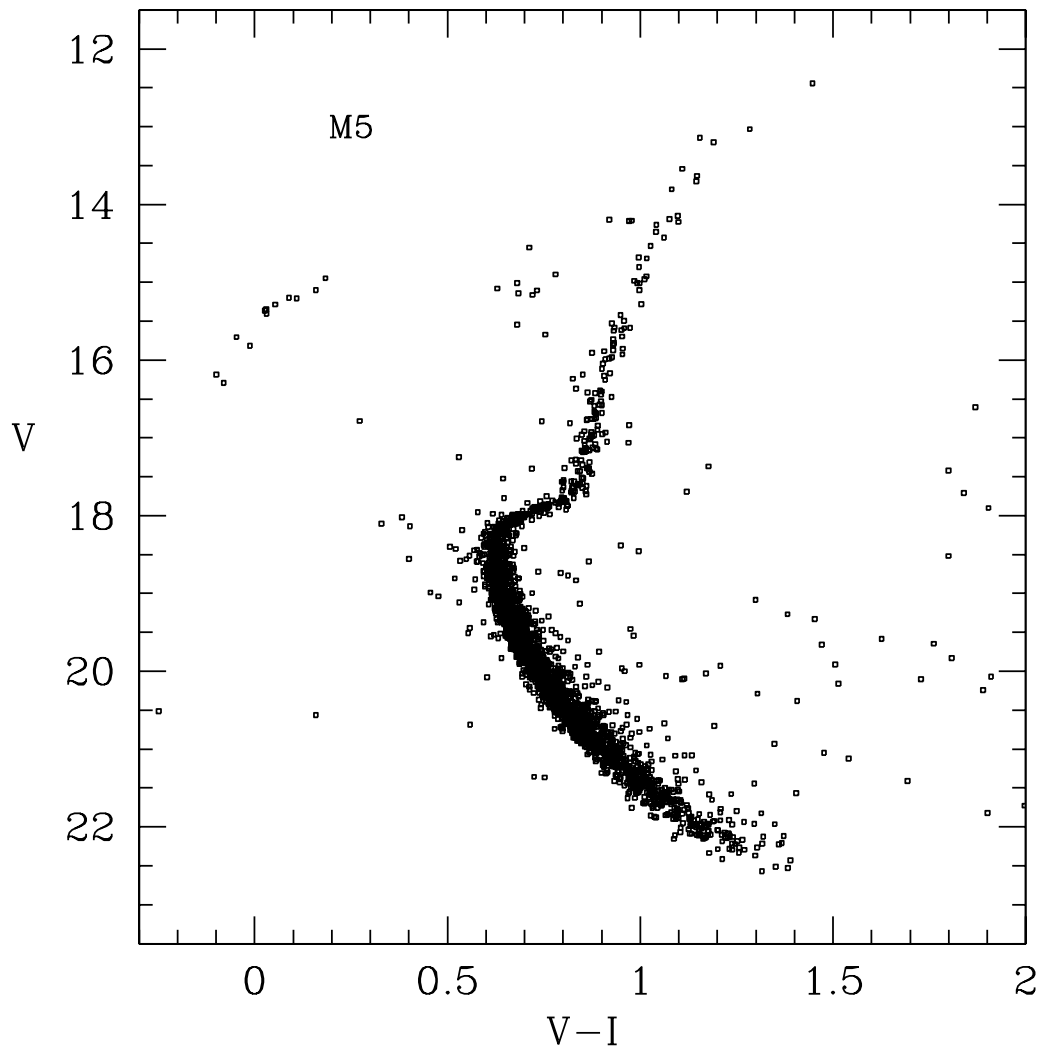
Stetson *et al.* --- Fig. 2



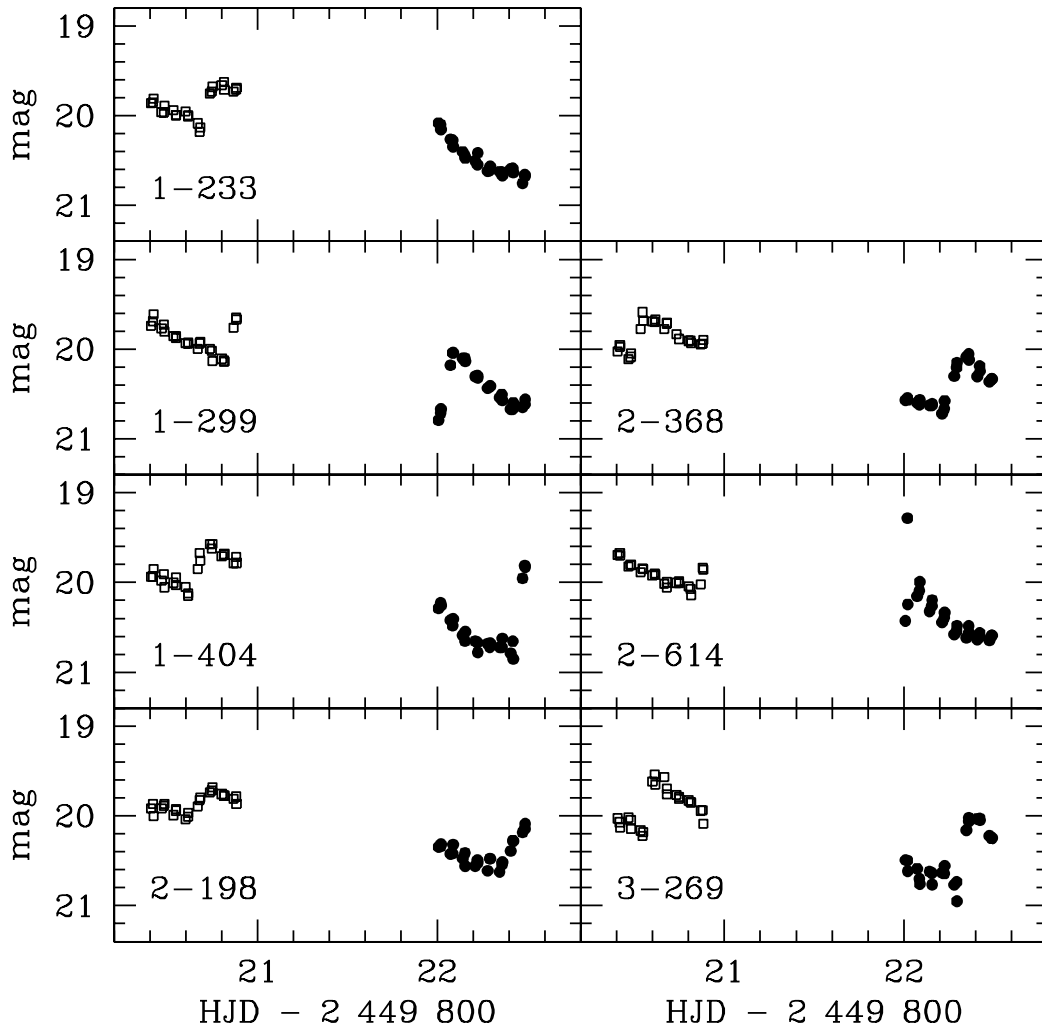
Stetson *et al.* --- Fig. 3



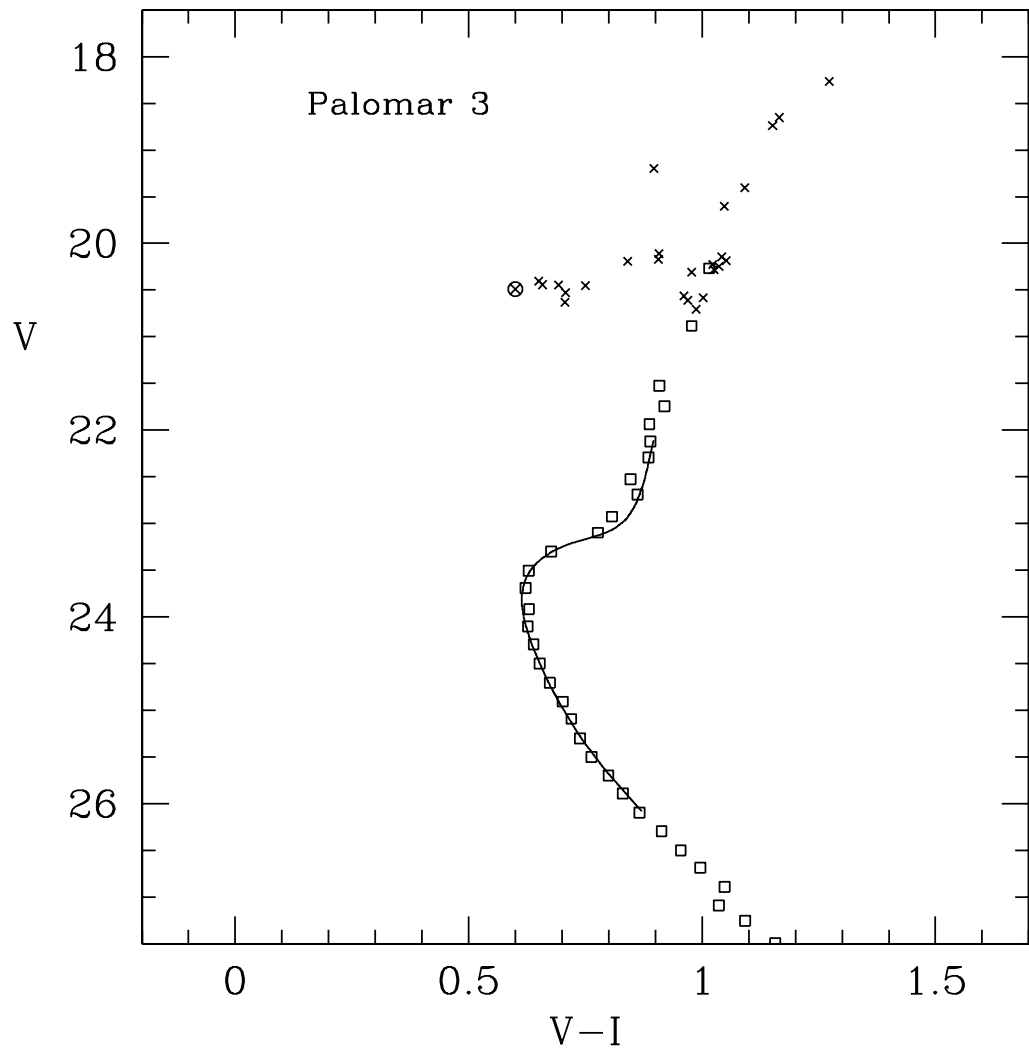
Stetson *et al.* --- Fig. 4



Stetson *et al.* --- Fig. 5

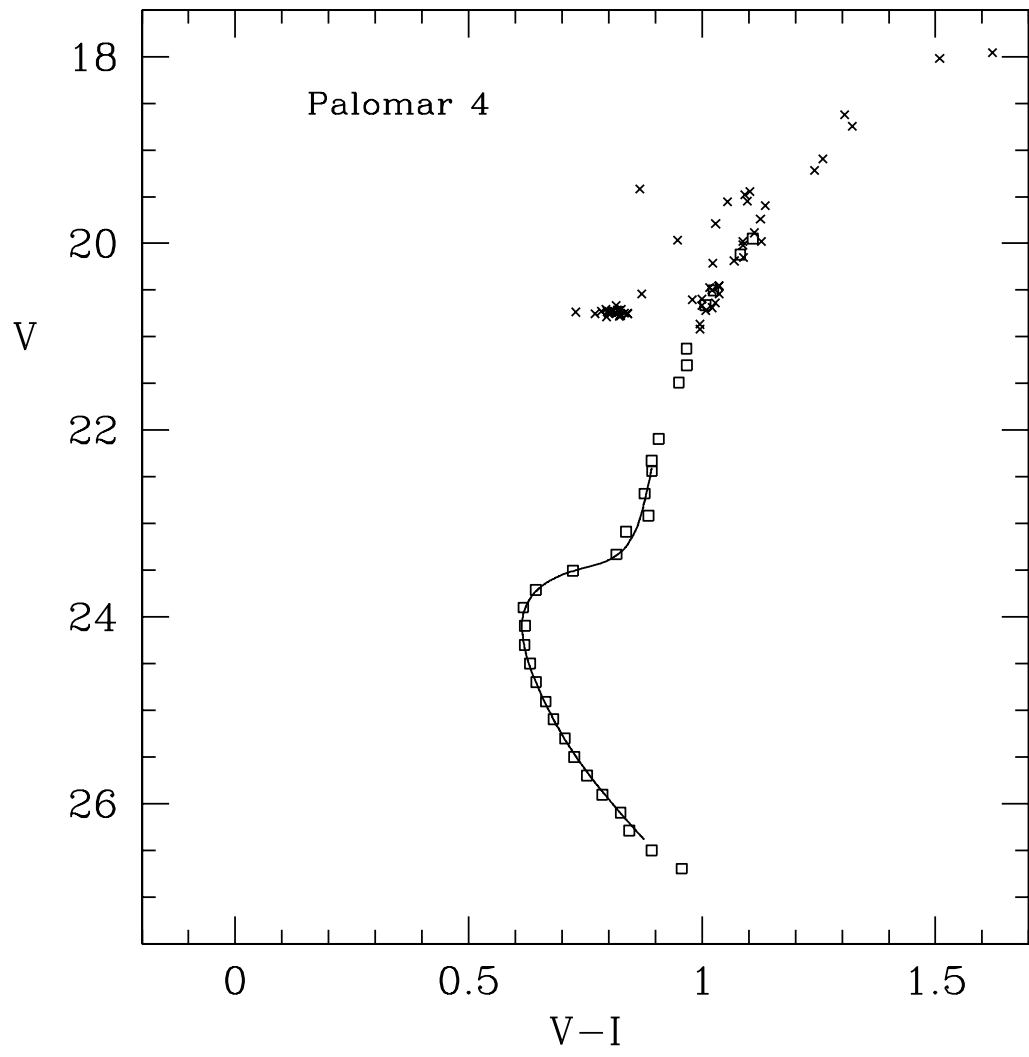


Stetson *et al.* --- Fig. 6

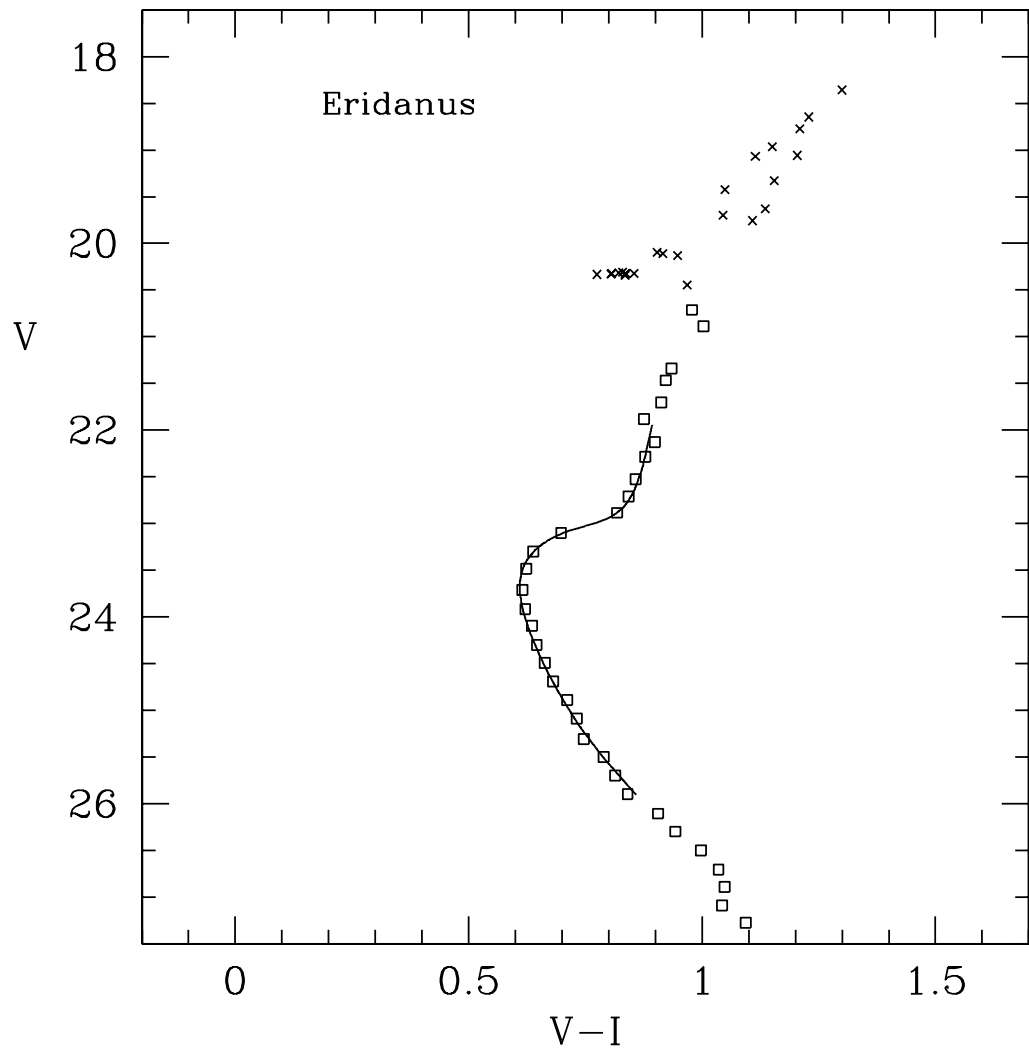


Stetson *et al.* --- Fig. 7

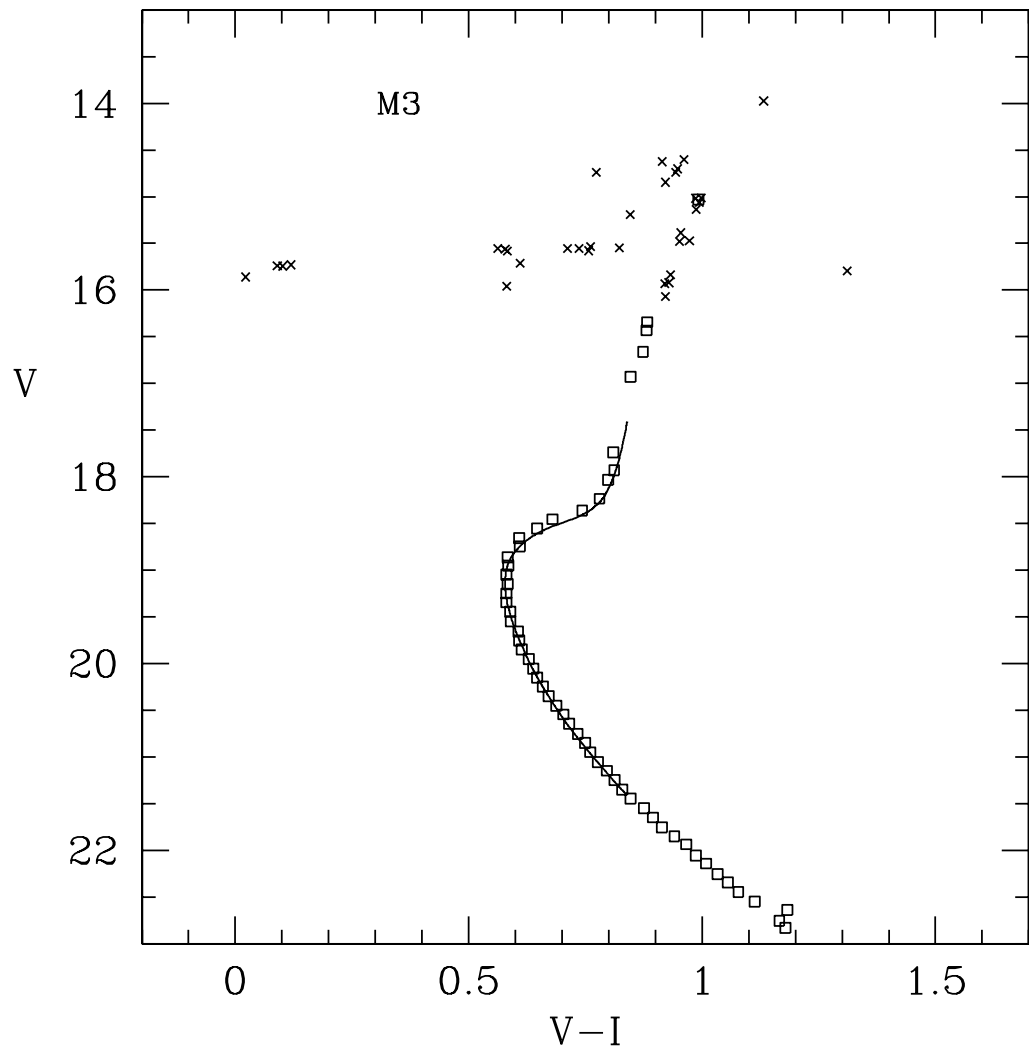




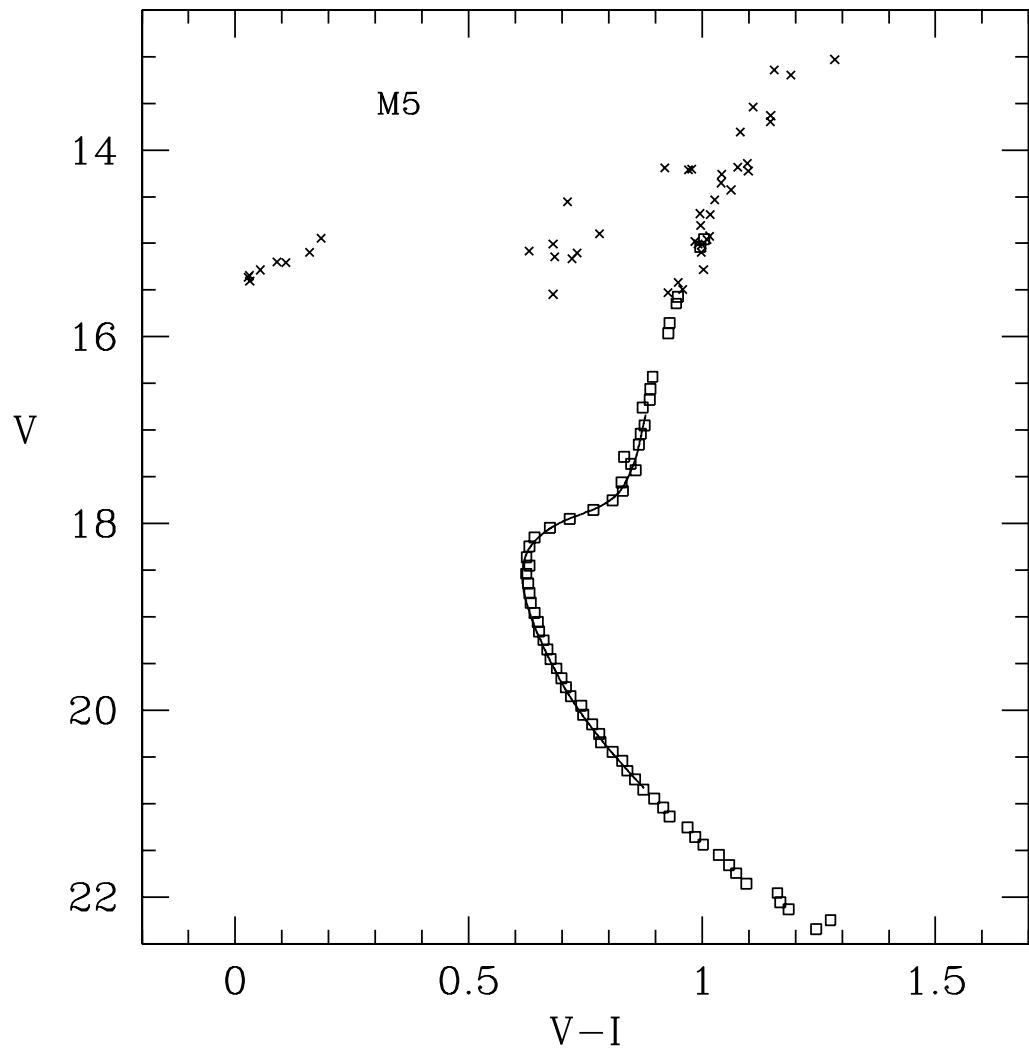
Stetson *et al.* --- Fig. 8



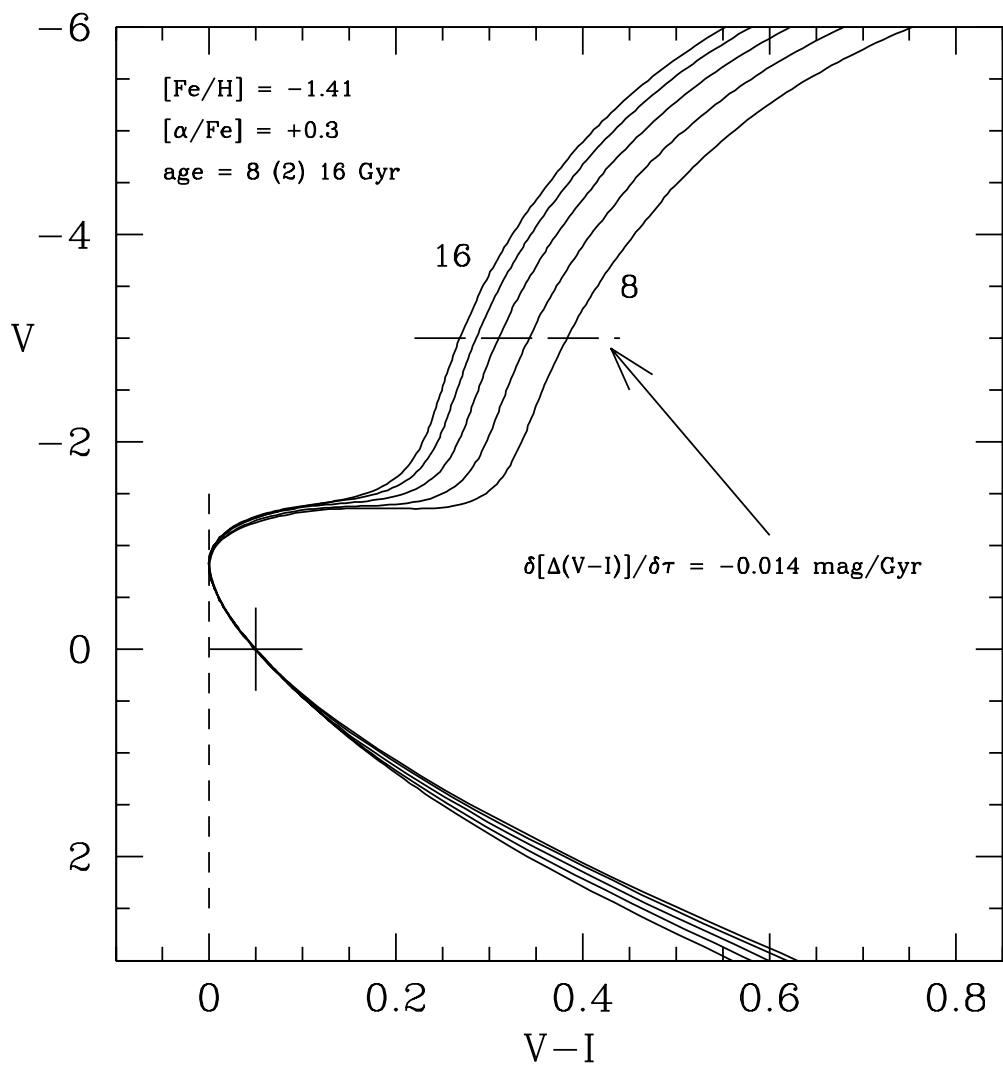
Stetson *et al.* --- Fig. 9



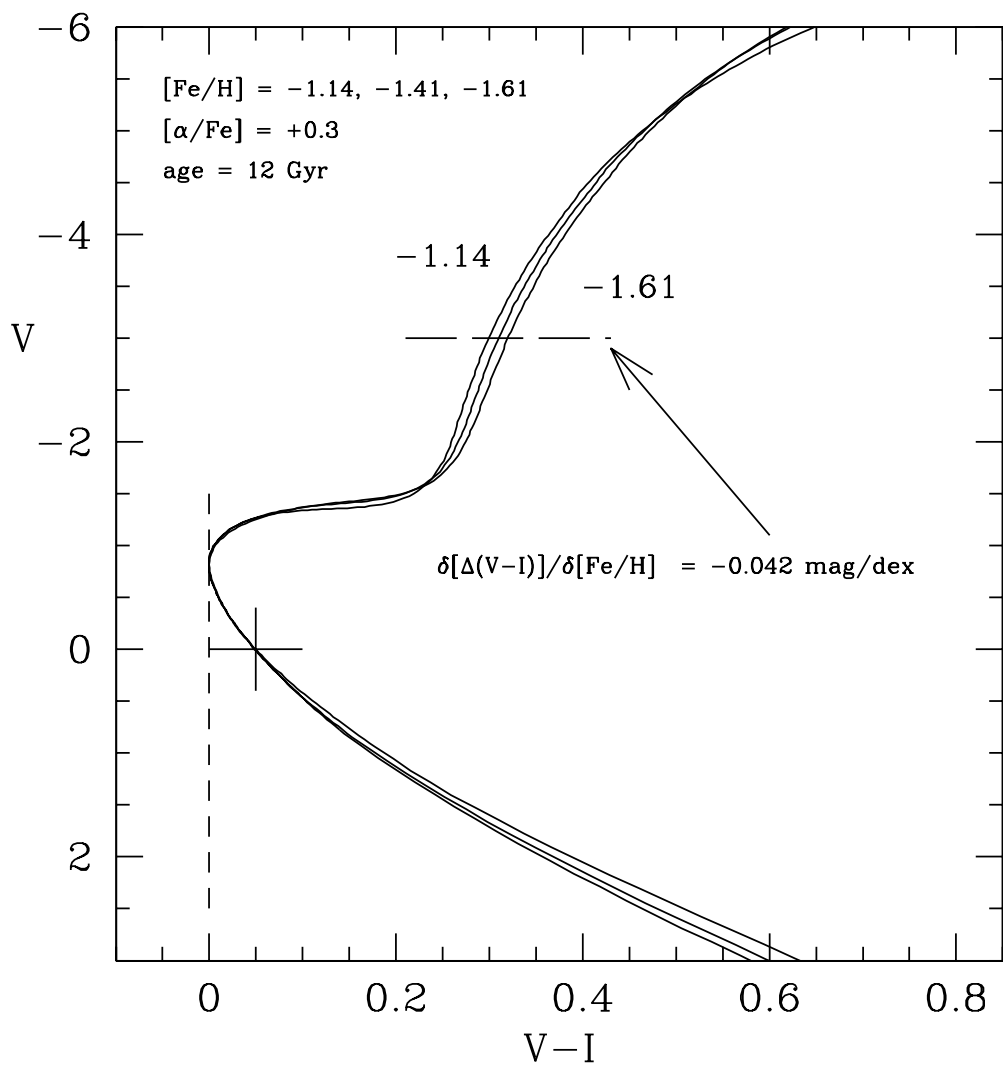
Stetson *et al.* --- Fig. 10



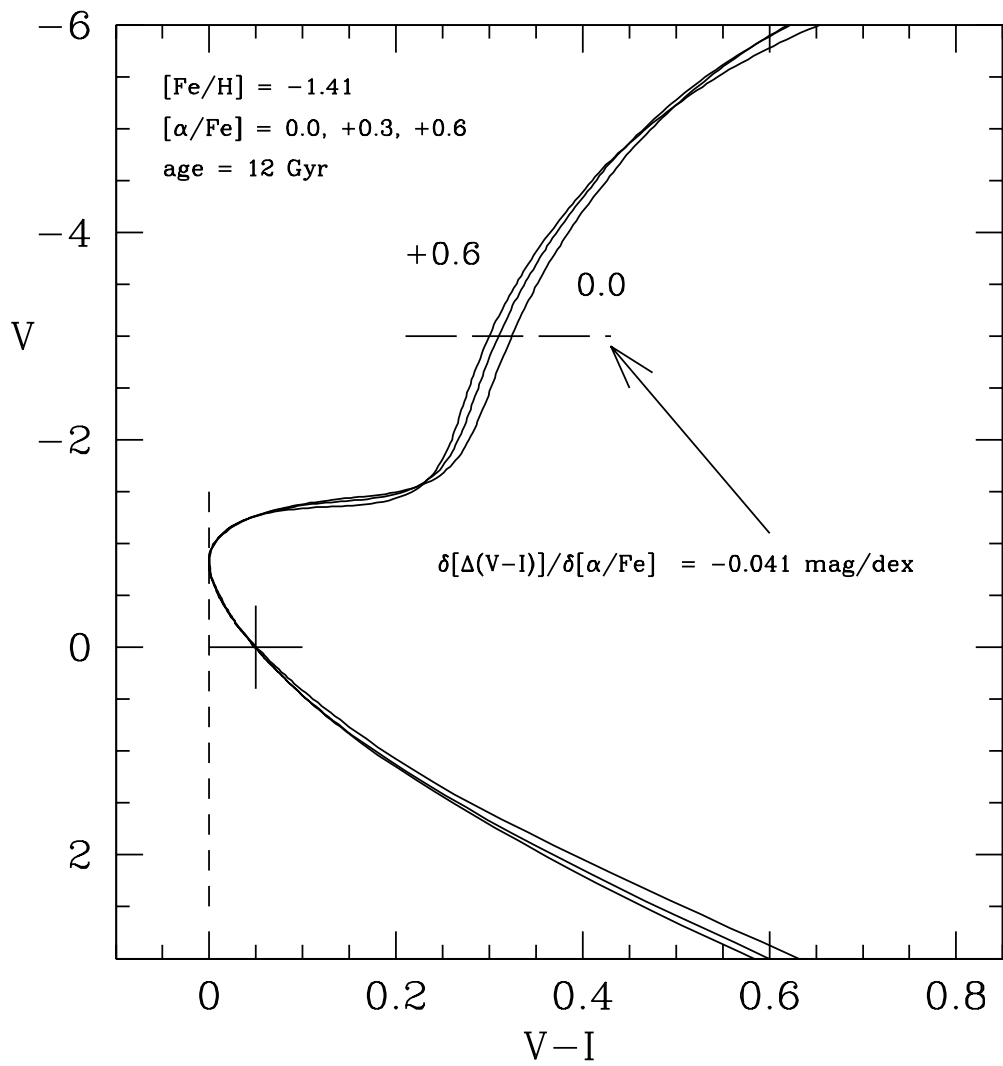
Stetson *et al.* --- Fig. 11



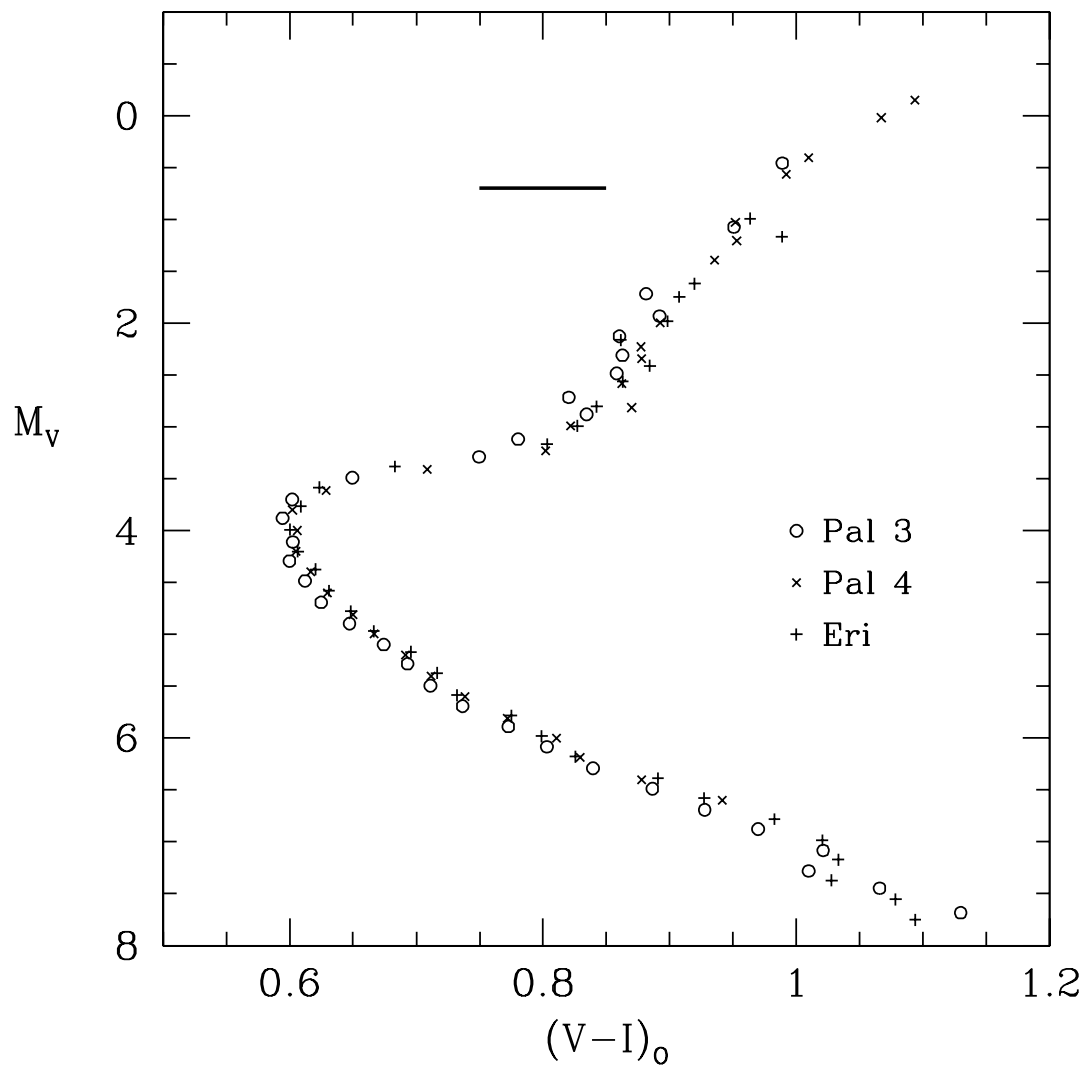
Stetson *et al.* --- Fig. 12



Stetson *et al.* --- Fig. 13

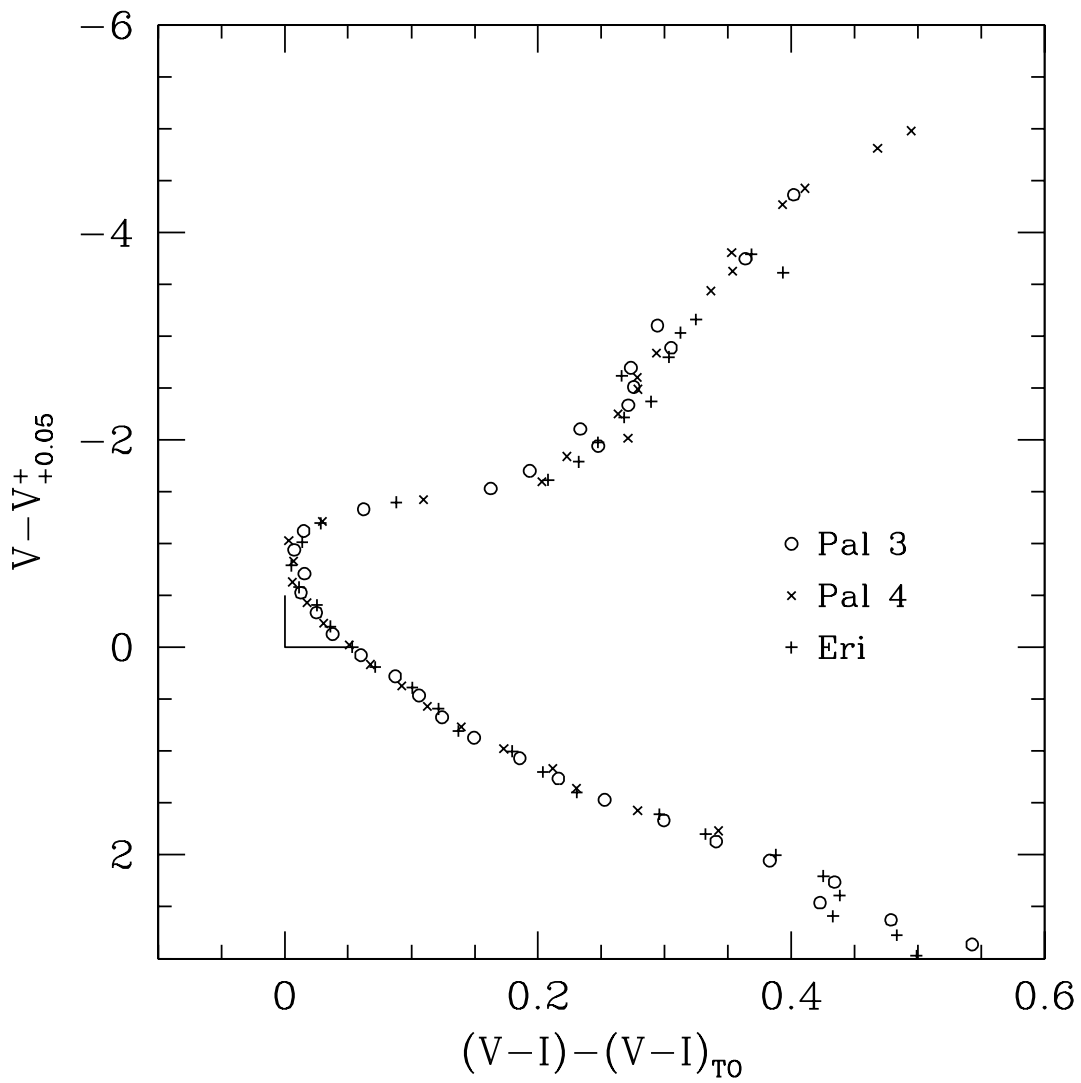


Stetson *et al.* --- Fig. 14

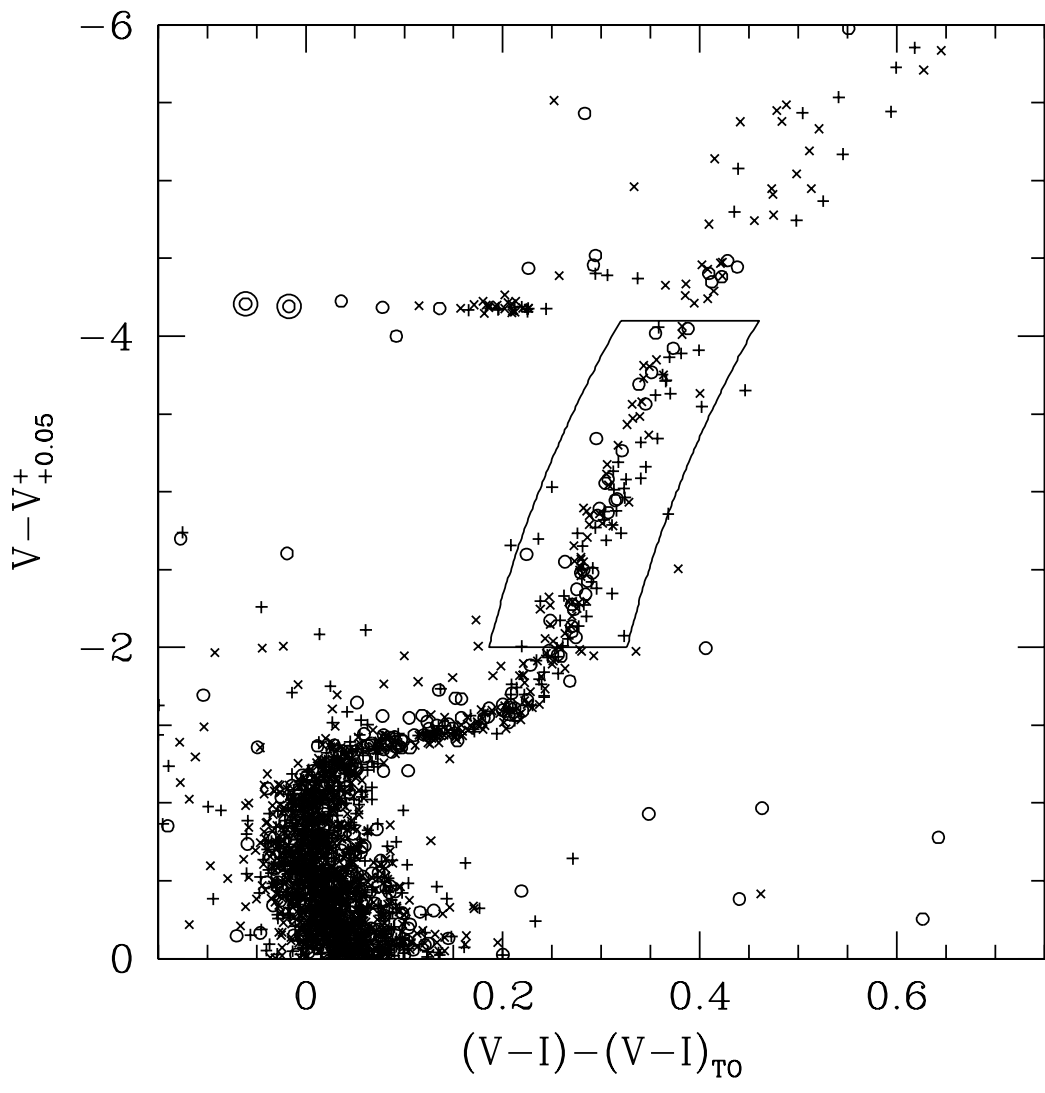


Stetson et al. --- Fig. 15

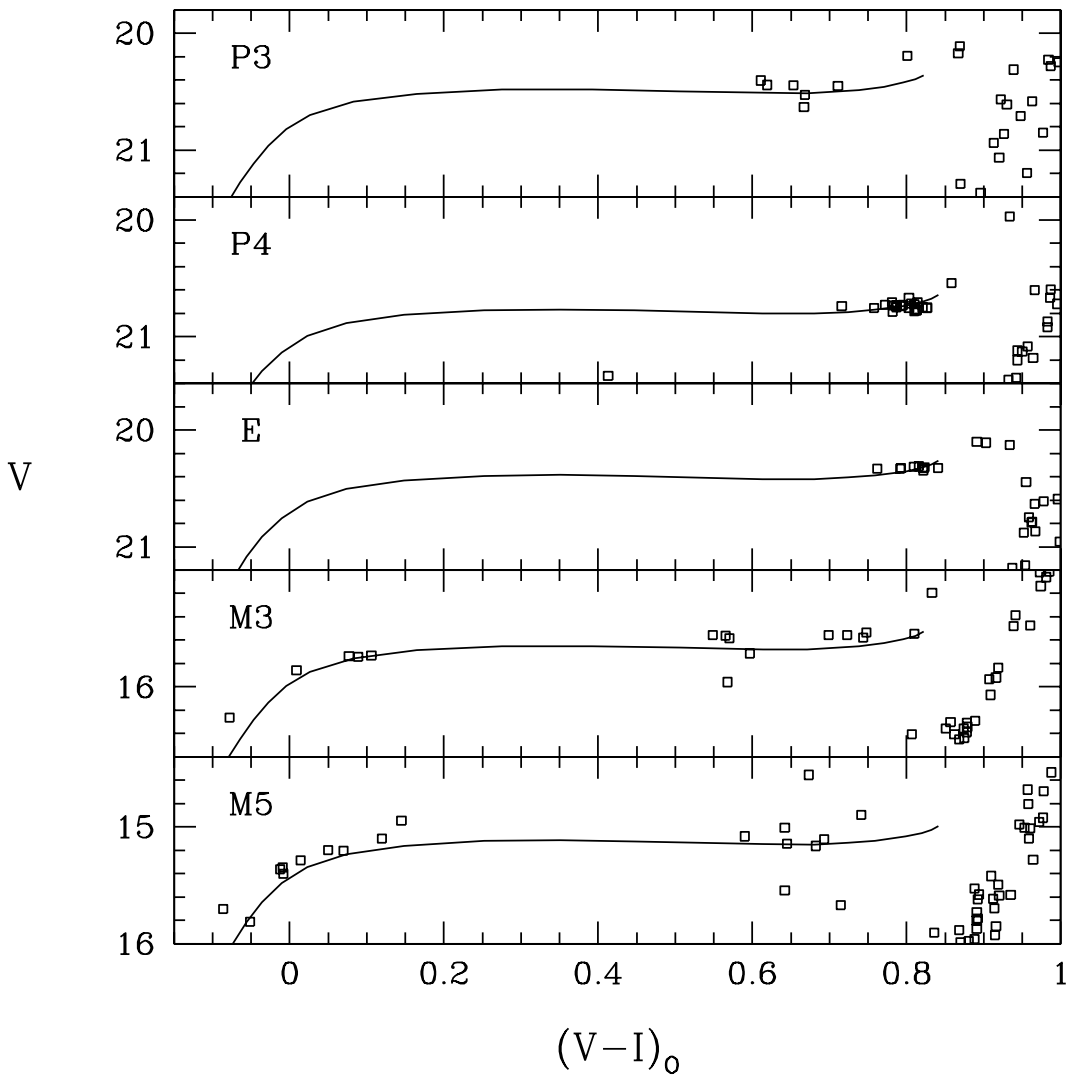




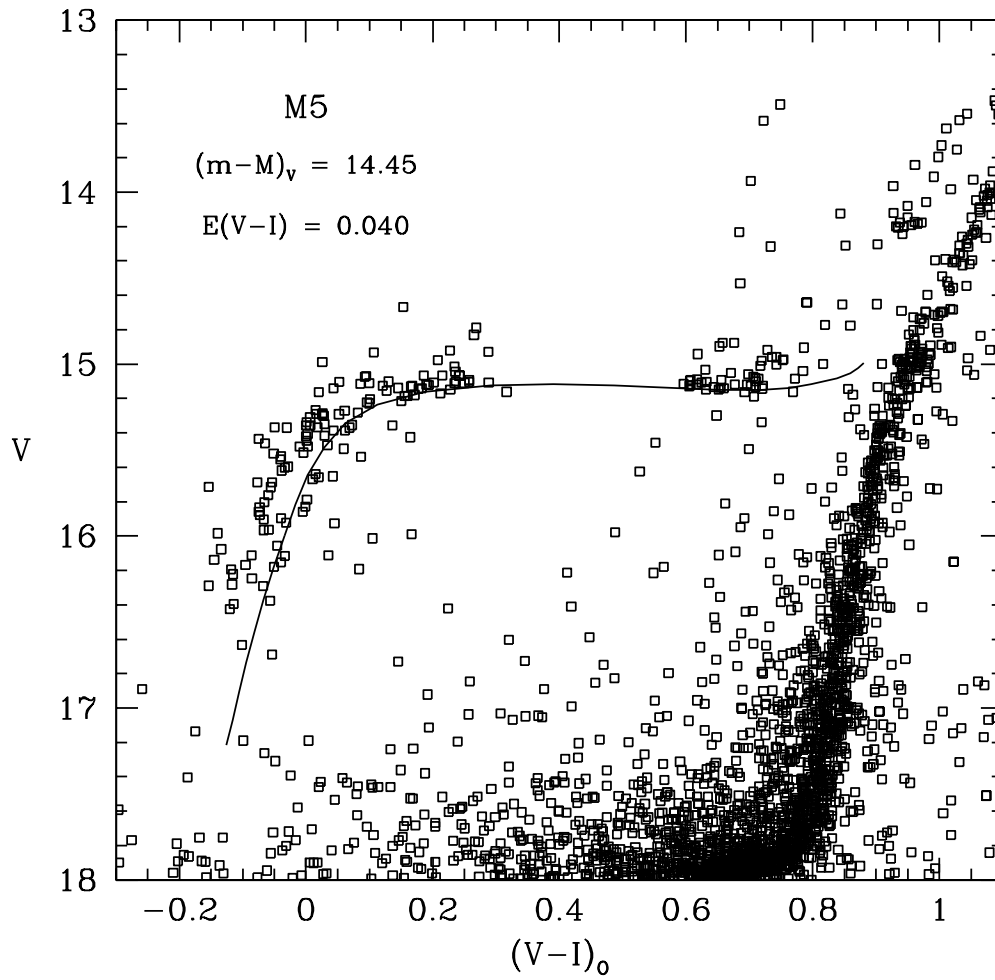
Stetson et al. --- Fig. 16



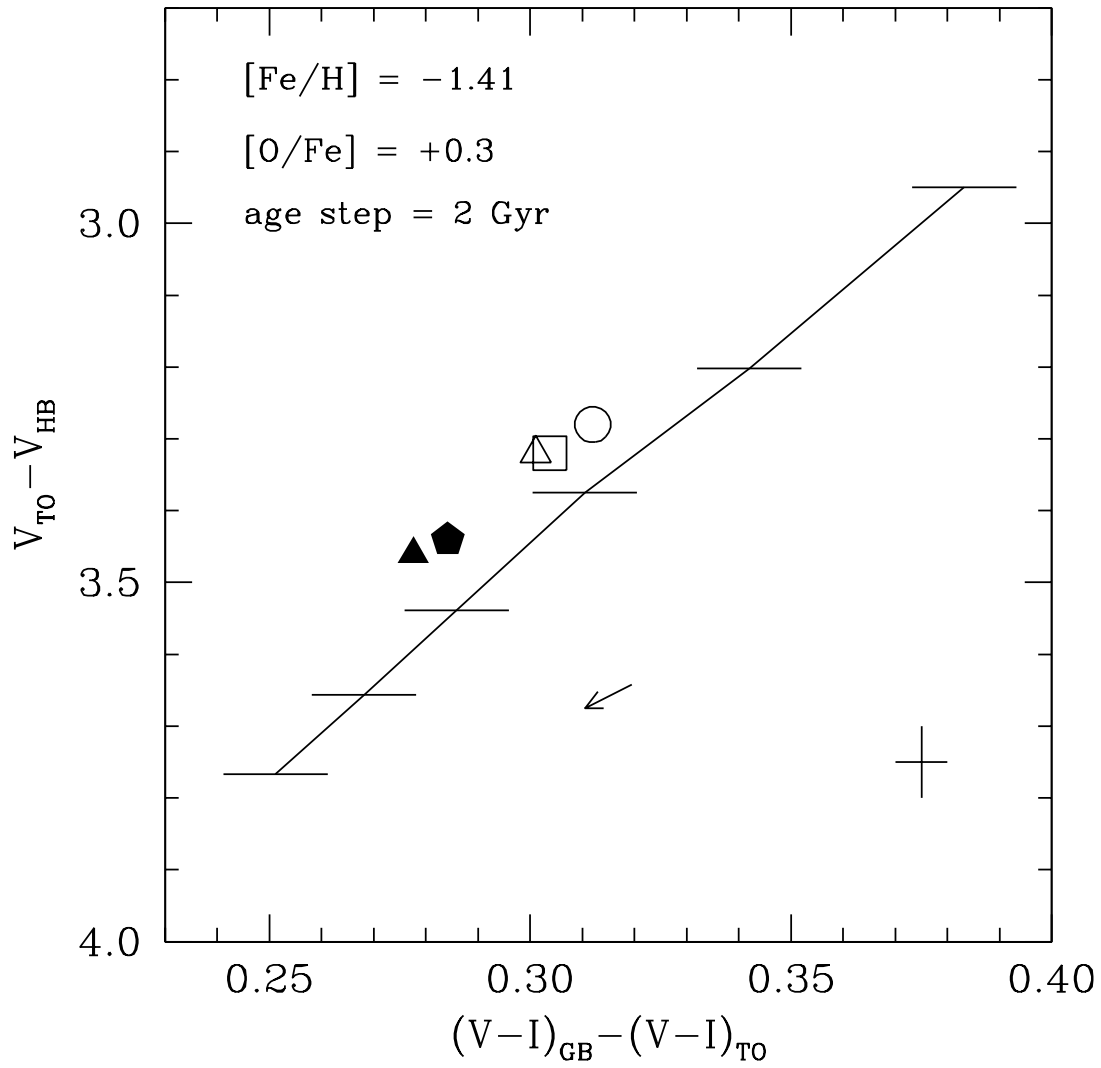
Stetson *et al.* --- Fig. 17



Stetson *et al.* --- Fig. 18



Stetson *et al.* --- Fig. 19



Stetson et al. --- Fig. 20